CHARACTERIZATION OF THE MIXING OF WHEAT STRAW SLURRIES THROUGH ELECTRICAL RESISTANCE TOMOGRAPHY (ERT)

by:

HIVA MOVAFAGH
B.Sc., Science and Research University, Tehran, Iran, 1999

A thesis

presented to Ryerson University

in partial fulfillment of the

Requirements for the Degree of

Master of Applied Science

in the Program of

Chemical Engineering

Toronto, Ontario, Canada, 2013

AUTHOR'S DECLARATION

I hereby declare that I am the sole author of this thesis. This is a true copy of the thesis, including any required final revisions, as accepted by my examiners.

I authorize Ryerson University to lend this thesis to other institutions or individuals for the purpose of scholarly research.

I further authorize Ryerson University to reproduce this thesis by photocopying or by other means, in total or in part, at the request of other institutions or individuals for the purpose of scholarly research.

I understand that my thesis may be made electronically available to the public.

ABSTRACT

Characterization of the Mixing of Wheat Straw Slurries through Electerical Resistance Tomography (ERT)

by:

Hiva Movafagh
Master of Applied Science
Chemical Engineering
Ryerson University
©2013

Wheat straw is a good source for the production of bioethanol. It can be converted into smaller fibers using mechanical treatment such as milling and grinding. These fibers can then be suspended in water and the slurry behaves as a non-Newtonian fluid possessing yield stress. In mixing operations, the presence of yield stress creates a region of active motion (called cavern) around the impeller, and stagnant zones in the rest of the tank. 2D and 3D electrical resistance tomography (ERT) images of wheat straw slurries were used in this study to measure the cavern diameter and height, respectively, created by mixing the slurries, and to estimate their yield stress from these dimensions. The average yield stresses of 5, 7, and 10 wt% slurries were 1.31 Pa, 4.2 Pa, and 14.8 Pa, respectively, when fiber size was $\leq$ 2 mm, and 3.4 Pa, 6.8 Pa, and 16.7 Pa, respectively, when fiber size was 8 mm $\pm$ 0.014 mm. The author believes that this study is the first novel application of ERT to estimate the yield stress of wheat straw slurries, as opposed to directly measuring it with a rheological instrument.

ACKNOWLEDGMENTS

I would first like to express my sincere gratitude and appreciation to my supervisors Dr. Farhad Ein-Mozaffari and Dr. Ginette Turcotte for their guidance and encouraging enthusiasm during all times of this work.

I acknowledge the assistance of all the staff and technologists in the Chemical Engineering Department at Ryerson University.

I also would like to acknowledge the advice and helpful suggestion of my friends in the Fluid Mixing Technology Laboratory at Ryerson University.

To Saeed

For his love and support

and

To my daughter and son, Soha and Illia

TABLE OF CONTENTS

LIST OF TABLES

LIST OF FIGURES

INTORDUCTION

Mixing of non-Newtonian fluids in stirred vessels is a common operation encountered in the chemical, biochemical, pharmaceutical, polymer, mineral, food, and wastewater treatment industries. A main group of non-Newtonian fluids exhibits the shear–thinning behaviour with yield stress (Skelland, 1967), such as pulp suspensions, certain polymers, biopolymer solutions, and wastewater sludge (Etchells *et al*., 1987). The shear-thinning fluids have low apparent viscosities at high shear rates and high apparent viscosities in low shear rates.

The design of the mixing systems for non-Newtonian fluids is more challenging than for Newtonian fluids due to the complex rheology of non-Newtonian fluids. Mixing of fibrous suspensions, which are non-Newtonian fluids with a yield stress, causes a well-mixed zone around the impeller called cavern with stagnant regions elsewhere (Wichterle and Wein, 1975). The stagnant regions within the mixing vessel result in ineffective heat and mass transfer (Amanullah *et al.*, 1997). To improve the mixing efficiency of a reactor, it is always beneficial to eradicate such undesired stagnant zones in the mixing of non-Newtonian fluids with yield stress.

The size of the cavern has significant effect on the mixing quality. Numerous experimental techniques, such as laser Doppler anemometry (LDA), X-ray photography, hotwired anemometry (HWA), planner laser induction (Arratia *et al*., 2006), ultrasonic Doppler velocimetry (UDV), positron emission particle tracking (PEPT) and electrical

resistance tomography (ERT), and the numerical technique called computational fluid dynamics (CFD) have been applied to study the formation of cavern generated in the mixing of yield stress fluids.

In the literature, there seems to be no study on the cavern evaluation of wheat straw suspensions. The recent and rapid development of non-intrusive ERT seems to provide an efficient tool for the analysis and control of mixing processes especially in the case of non-Newtonian fluids (either opaque or transparent). Electrical resistance tomography (ERT), which is an emerging technology, can be the best alternative to measure the cavern size and to analyze fluid flow in 2D and 3D.

This study will try to employ ERT to study the mixing of wheat straw slurries, which are yield–pseudoplastic fluids, with the A200, A310, and A100 impellers in terms of cavern shape and size. In this study, for the first time, the yield stress of the wheat straw slurries was estimated by applying the cavern size obtained from ERT tomograms.

CHAPTER 1

LITERATURE REVIEW

1.1 *Wheat Straw*

Wheat straw is an agricultural residue made of stalks, stem, and dried leaves of the wheat plant. It contains about 58-78 wt % total sugars depending on the species (Himmel *et al*., 2007).

International wheat production statistics from years 2000 to 2010 show that wheat straw is the largest biomass feed stock in Europe (FAOSTAT Database, 2011). More than 21% of the world's food depends on the wheat crop, so, in order to satisfy the great demand of human's need, the production of wheat crop need to be increased.

Wheat straw is a complex mixture of three main components: cellulose, hemicellulose and lignin. Generally, wheat straw contains of 33-40 (wt%) of cellulose, 20-25 (wt%) of hemicellulose, and 15-20 (wt%) of lignin (Prasad *et al*., 2007). Cellulose is a linear mono-polymer chain comprised of D-glucose units attached to each other via β-1→ 4-glycosidic bonds. Hemicellulose consists of long chain of xylose molecules, etc. Lignin is an amorphous polymer consisting of phenylpropane units, and it has three aromatic alcohols (monolignols) precursors of *p*-coumaryl, coniferyl and sinapyl alcohols, which are shown in Figure 1.1 (Buranov and Mezza , 2008).

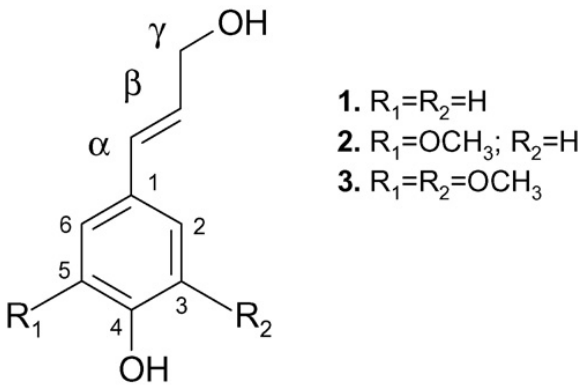

Figure 1.1. Lignin monolinguols

Lignocellulosic materials are a good source for ethanol production (Taherzadeh and Karimi, 2007). The main objective of this chapter is to conduct a literature review on the mixing performance in wheat straw, which is applied in ethanol production. This literature review includes the ethanol production process, wheat straw suspension rheology, power consumption, impeller type, and cavern formation; finally, some ERT applications in mixing are presented.

1.1.1 Ethanol Production from Wheat Straw

Wheat straw is the most attractive low cost feedstock for production of fuel alcohol due to its abundance, renewability and low lignin content (Buranov and Mezza, 2008). Numerous studies were done on the bioconversion of lignocellulose to produce ethanol (Erdei *et al*., 2010; Talebnia *et al.*, 2009; Kaparaju *et al*., 2009) . This process contains three steps: (1) pre-treatment, to break down the recalcitrant structures of lignocellulose; (2) hydrolysis, to hydrolyze polysaccharides (e.g., cellulose, hemicellulose) into

fermentable sugars; and (3) fermentation, to convert sugars into ethanol (Hahn-Hagerdal *et al.*, 2006; Jorgensen *et al.*, 2007).

1.1.1.1 Pre-treatment

Pre-treatment is a significant process in the utilization of lignocellulosic material to achieve large amounts of fermentable sugars. Pre-treatment is performed to break the lignin seal, decrease crystallinity of the cellulose and solubilize hemicellulose (Patel *et al.*, 2009). Pre-treatment techniques are categorized in four groups of physical, chemical, physicochemical, and biological.

Physical pre-treatment: chipping, milling and grinding are main types of physical pre-treatments. These treatments reduce both the crystallinity and the degree of polymerization (DP) of cellulose. In addition, they increase the specific surface area (Sun and Cheng, 2002).

Chipping reduces the biomass size to 10–30 mm while grinding and milling can decrease the particle size to 0.2–2 mm. Particle size and cellulose crystallinity are reduced in grinding and milling more than chipping probably because of the shear forces created during milling and grinding. Increasing specific surface area and reducing both cellulose crystallinity and degree of polymerization (DP) are all dependent on the type and duration of milling as well as the type of biomass.

Chemical pre-treatment: chemicals such as acids, alkali, cellulose / organic solvents, and ionic liquids can affect lignocellulosic biomass structure (Swatloski *et al*., 2002). In acid pretreatment (typically H_2SO_4), most of the hemicellulose is removed and converted to soluble sugars (Gil *et al*., 2010; Guo *et al*., 2008). Alkali pre-treatment such as NaOH,

KOH, $Ca(OH)_2$, hydrazine and anhydrous ammonia can break the lignin structure, increase the internal surface of biomass and reduce both the degree of polymerization and crystallinity (Chandra *et al*., 2007; Chang and Holtzapple, 2000; Galbe and Zacchi, 2007). The most effective chemical pre-treatment for biomass with low lignin content such as wheat straw is alkali pre-treatment (Agbor *et al*., 2011). Combined cellulose/organic solvent pre-treatment separates lignocellulose components by using a cellulose solvent such as concentrated phosphoric acid, organic solvent like acetone, and water (Zhang *et al.,* 2007; Zhu *et al.,* 2009). Ionic liquids (ILs) have been used as novel non-derivatizing media for the dissolution of carbohydrates including cellulose (Swatloski *et al.,* 2002; Zhao *et al.,* 2008). Many ILs, especially those containing halide, acetate, formate, and phosphate anions, dissolve cellulose quickly (Ohno and Fukaya, 2009).

Physicochemical pre-treatment: physicochemical pre-treatments are combinations of physical and chemical pre-treatments. They include steam pre-treatment (or steam explosion), liquid hot water pre-treatment, wet oxidation pre-treatment, ammonia fiber expansion (AFEX), ammonia recycle percolation, aqueous ammonia pre-treatment and organosolv pre-treatment (Zhu *et al.,* 2006; Zhu *et al.,* 2009).

Biological pre-treatment: fungi are used in biological pre-treatment. Fungi are able to produce enzymes that degrade lignin, hemicellulose, and polyphenols. White and soft-rot fungi are capable of degrading lignocellulose material. However, brown rot fungi can degrade cellulose structure. White-rot fungi are known as the most effective biological pre-treatment (Lee, 1997; Sun and Cheng, 2002). This method is not used in industry due

to several factors such as the need for careful growth environment, a residence time of 10–14 days and the need of large biological reactors (Agbor *et al.*, 2011).

1.1.1.2 Hydrolysis

Enzymatic Hydrolysis

Cellulose slowly degrades into glucose by a group of enzymes (cellulases) with various functions during enzymatic hydrolysis of pre-treated lignocellulosic biomass. Cellulase refers to a group of enzymes produced by fungi, bacteria, and protozoans that catalyze cellulolysis (i.e. the hydrolysis of cellulose) (Watanabe *et al.*, 2010). All these enzymes can hydrolyze cellulose by creating new attainable sites for each other. The incomplete conversion of cellobiose to glucose and inhibition of cellobiohydrolase (CBH) are happening because *Trichoderma reesei* secretes low levels of β-glucosidase enzyme. Therefore, in order to obtain complete conversion of cellobiose to glucose, it is always required to use supplemental β-glucosidase, such as Novozyme 188 as shown in Table 1.1 (Zhang *et al.*, 2010; Kumar and Wyman, 2009).

Acid Hydrolysis

Dilute acid hydrolysis is also another way to cleave ether bonds between hemicellulose and lignin complexes. Dilute acid (0.75% H_2SO_4) at 120–180 °C can both solubilize hemicellulose and convert solubilized hemicellulose to fermentable sugars (Grohmann *et al*., 1985; Saha *et al*., 2005). Studies show that during the organosolv and aqueous ethanol delignification of wheat straw, a major factor in lignin breakdown is the cleavage of α-

aryl and β-aryl ether linkages in lignin precursors. The cleavage of α-aryl ether bonds is faster than that of β-aryl ether bonds when acid catalyst is added (Papatheofanous *et al.*, 1998; Xu *et al.*, 2006; Hongzhang and Liying, 2007). Experiments show that during organosolv pulping of wheat straw in presence of formic–acetic acid–water (30/60/10) system, more than 94.1% of original lignin is removed (Xu *et al.*, 2006).

Table 1.1. Summary of some multi-enzyme complexes and the role of supplemental enzymes

Multi-enzyme complex	**The role of supplemental enzymes**	**Reference**
Cellulase+β-glucosidase	Eliminate the inhibition of cellobiose to cellulase	Zhang *et al*., 2010 and Kumar and Wyman, 2009
Cellulase+β-glucosidase+xylanases	Hydrolyze the xylan and make the cellulose more accessible to cellulase	Zhang *et al*., 2010 ; Kumar and Wyman, 2009; Berlin *et al*., 2007
Cellulase+β-glucosidase+pectinases	Remove the pectin that coat cellulose fibers	Zhang *et al*., 2010 and Berlin *et al*., 2007
Cellulase+xylanase+β-xylosidase	Hydrolyze the xylan and eliminate the inhibition of xylobiose and higher xylooligomers	Kumar and Wyman, 2009
Cellulase+endoxylanase+α-L-arabinofuranosidase	Remove the arabinofuranosyl group that limits the access of xylanases to xylan backbone	Sorensen *et al*., 2007 and Alvira *et al*., 2011

1.1.1.3 Fermentation

Ethanol fermentation is a biological process in which sugars such as glucose, xylose, and sucrose are converted into cellular energy and thereby produces ethanol and carbon dioxide as metabolic waste products. Several studies have been done to develop efficient pentose (especially xylose) fermenting microorganisms, such as recombinant *Saccharomyces cerevisiae*, *Zymomonas mobilis* and *Escherichia coli* strains (Hahn *et al.*, 2007; Yonge *et al*., 2010).

Figure 1.2 shows three main strategies for strain improvement in cellulosic ethanol production; (1) pentose utilization, (2) direct cellobiose fermentation and (3) tolerance enhancement (Renliang *et al*., 2011).

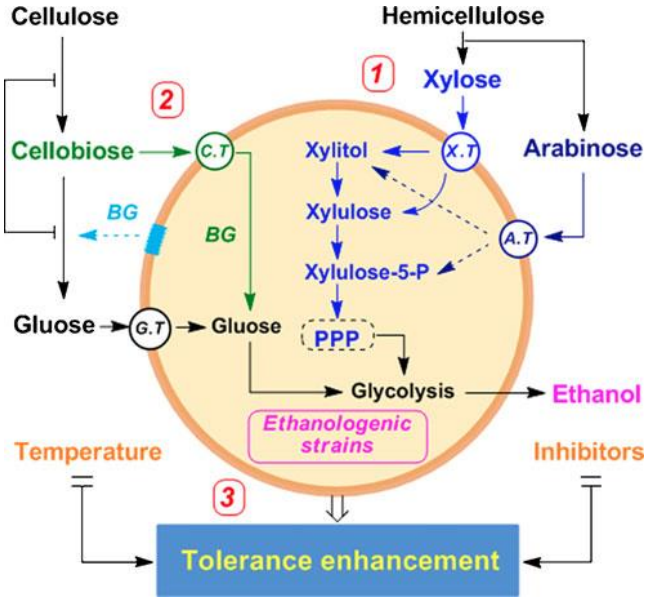

Figure 1.2. Three main strategies for strain improvement in cellulosic ethanol production

Literature reviews show that one of the important steps for the fermentation of xylose to ethanol is the transport of xylose in *S. cerevisiae* especially at low xylose concentrations. This transport is significant because it appears through nonspecific hexose transporters. Recently, some heterologous xylose transporters have been found in recombinant *S. cerevisiae*. These transporters such as Gxf1 (Hagerdal, 2009), Sut1 (Katahira *et al*., 2008) are used to increase the absorption of xylose. Ethanologenic microorganisms are useful to convert cellulosic biomass into ethanol (Figure 1.2). There are two ways to convert cellulosic biomass into ethanol. The first way is to use both cellobiose transporter and intracellular β-glucosidase into microorganisms (Galazka *et al*., 2010) while the second way is to produce extracellular β-glucosidase from ethanologenic microorganisms (Nakamura *et al*., 2008).

1.2 *Wheat Straw Suspension Rheology*

One important factor in the mixing of non-Newtonian fluids is the rheological behaviour of the fluid (Pakzad *et al.,* 2008). Rheology is the study of deformation and flow of matter, especially in soft solids and liquids with a complex flow behavior (Viamajala *et al*., 2009). The rheological behavior is significant in the pulp and paper and in the biomass processing industries.

Some studies have been done so far on the rheological properties of cellulose fiber suspensions (Chaussy *et al*., 2011; Derakhshandeh *et al*., 2010; and Hui *et al*., 2009) and

also pre-treated lignocellulosic materials, especially corn stover (Primenova *et al*., 2004). Yield stress is one of the most important rheological properties of pulp suspensions in designing process equipment for the pulp and paper industry (Derakhshandeh *et al*., 2011). The yield stress of a fiber suspension is a key parameter in pulp manufacturing since the suspension flows once the yield stress is overcome.

Rheological studies on the slurries of pre-treated corn stover and various pulp fibers have also shown that the yield stress is a function of the fiber mass concentration through a power-law relationship as shown in Equation (1.1) (Lavenson *et al*., 2011):

$$\tau_y = aC_m^b \tag{1.1}$$

where *a* and *b* are empirical constants. Lavenson *et al*. (2011) compared fiber types to observe the direct effect of fiber properties on rheology.

Bennington *et al*. (1990) measured the yield stress of pulp and synthetic fiber suspensions using an equation based on network theory, which included fiber aspect ratio and Young's modulus:

$$\tau_y = cEA^2C_v^3 \tag{1.2}$$

where A is the fiber aspect ratio, E is the fiber's Young's modulus, c is a constant and C_v is the volume concentration of the pulp suspension.

Chen *et al*. (2002) studied the flow behavior of pulp suspensions and identified three flow regimes. In the first regime, Newtonian flow was observed at low shear rates. Unstable flow was found in the second region, with jumps in the shear stress dependent on shear rate. In the third region, Newtonian behavior at high shear rates was observed, which was called dynamic equilibrium zone. This kind of behavior requires a flexible mixing system to cover the wide range of rheological behavior.

Hui *et al*. (2009) studied pulp fiber suspensions with concentrations from 1.0 wt% to 5.0 wt%. They found that the pulp fiber suspensions displayed non-Newtonian rheological behavior with yield stress. This finding was in contrast with Chen *et al*. (2002), who mentioned that the rheological behavior of pulp suspension is flow dependent.

Derakhshandeh *et al*. (2010b) studied the flow behavior of 0.5-5.0 wt% of pulp suspensions, using both conventional and coupled UDV-rheometry techniques. They observed that by increasing the fiber mass concentration, the apparent yield stress and the consistency index (*K)* in the Herschel-Bulkley model increased, while the power–law index (*n*) in the Herschel-Bulkley model decreased. They explained that these materials show a Newtonian behavior at high shear rates, which is referred to the turbulent regime. The shear stress values at which this regime begins were measured and reported as the critical shear stress for the onset of turbulence.

Chaussy *et al*. (2011) examined the rheological behavior of fiber suspensions using the Carreau-Yasuda model. This model does not show discontinuities and enables the description of the pulp suspensions behavior for the entire domain of shear rates up to 2.1 $\times$ 10^{6} s^{-1}. They concluded that the pulp suspensions behave as a Newtonian fluid at the

lower shear rates and as a shear thinning fluid at the higher shear rates. They also observed that the suspension viscosity increased with fiber concentration, fiber length, and pH of the suspension.

Viamajala *et al*. (2009) examined the rheology of acid hydrolyzed corn stover at concentrations between 10.0-40.0 wt%. These slurries behaved like yield stress fluids. With increasing hydrolysis temperature and decreasing particle size, the yield stress decreased. They believed that with solids concentration up to a point, yield stress increased and then became independent of concentration at the high concentrations. The reason for the plateau at high concentrations is not clear.

The study of pre-treated lignocellulose (sawdust slurries) by Dasari and Berson (2007) showed that the rheology of pre-treated lignocellulose is affected by the fiber size. They reported that the yield stress of the slurry increased with an increase in fiber length.

Rosgaard *et al*. (2007) investigated the effect of solids content and enzymatic hydrolysis on the apparent viscosity of barley straw biomass slurries, with solids mass fraction varying from 5 wt% to 15 wt%. It was proved in this study that the apparent viscosity increased with solids mass fraction, and decreased with time during enzymatic hydrolysis.

Bashir (2008) measured the rheological properties of wheat straw suspensions at concentrations between 5.0-20.0 wt%. Wheat straw fibers were made by grinding wet or dry wheat straw and were divided into four sizes: 8, 12, 20, and 40 mesh. The yield stress was found to increase with concentration as well as with the size of the wheat straw fibers as shown in Table 1.2. The yield stress data were fitted to the power law equation

proposed by Kerekes *et al*. (1985) for pulp fibers. It was found that only the yield stress of the slurry of 40 mesh size wheat straw fibers agreed with this power law correlation.

Table 1.2. Yield stress values at various concentrations of wheat straw for mesh sizes of 40, 20, 12 and 8

Concentration (%, w/v)	**Yield Stress(Pa)** (40 mesh)	**Yield Stress(Pa)** (20 mesh)	**Yield Stress(Pa)** (12 mesh)	**Yield Stress(Pa)** (8 mesh)
5	*	171	399	411
10	153	195	426	739
15	354	405	516	765
20	462	510	684	1035

*Sedimentation effect was prominent only in 5 wt% (40 mesh) wheat straw suspensions, where no yield stress was found (Bashir, 2008).

1.3 *Fiber Networks*

The large aspect ratio of pulp fiber brings significant contact among fibers (Derakhshadeh *et al*., 2011).This has a strong effect on suspension rheology. For fibers to form flocs or coherent networks, every fiber must be in contact with at least three other fibers (Dodson, 1996; Meyer and Wahren, 1964; Soszynski and Kerekes, 1988a). This contact regime has been described by a crowding number (N), which is the average number of fibers in a spherical volume swept out by the length of the single fiber (Kerekes et al., 1985).

The concentration of fiber suspensions can be characterized by the crowding number (Kerekes and Schell, 1992; Dodson, 1996).

Samaniuk *et al.* (2011) study showed that cellulose fibers in water form networks that give rise to an apparent yield stress, especially at high solids contents.

1.4 *Power Consumption*

Power consumption is a significant parameter for mixing system. It can be defined as the energy transformed from an impeller to a fluid per unit time (Tatterson, 1991). Having knowledge about power consumption is very important in order to operate the impeller **(**Chhabra and Richardson, 1999). The impeller power in a homogeneous liquid depends on the geometry of impeller and tank, the density and viscosity of the fluid, the impeller speed and the gravitational force as shown in the following equation (Tatterson, 1991):

$$P = f(\mu, \rho, N, D, T, g) \tag{1.3}$$

where P,μ, ρ, N, D, T, and g are power, fluid viscosity, fluid density, impeller speed, impeller diameter, tank diameter, and gravitational acceleration, respectively. Applying the dimensional analysis, Equation (1.4) is obtained (Skelland, 1967):

$$\frac{P}{\rho N^3 D^5} = f\left(\frac{\rho N D^2}{\mu}, \frac{N^2 D}{g}\right) = f(\mathrm{Re}, Fr) \tag{1.4}$$

This equation shows that the dimensionless power coefficient $P/\rho N^3 D^5$ depends on both Reynolds number and Froude number for a fluid. The dimensionless groups are as follows:

$$P_o = \frac{P}{\rho N^3 D^5} \tag{1.5}$$

$$Fr = \frac{DN^2}{g} \tag{1.6}$$

$$\mathrm{Re} = \frac{\rho N D^2}{\mu} \tag{1.7}$$

1.4.1 Power Requirements for Mixing of non-Newtonian Fluids

The key objective of any mixing process is to maximize the degree of homogeneity of a property such as concentration, viscosity, color, and temperature (Chhabra and Richardson, 2008). For a stirrer system and for a non-Newtonian fluid, the Reynolds number is defined as Equation (1.8):

$$Re = \frac{\rho N D^2}{\mu_{app}} \tag{1.8}$$

In non-Newtonian fluids, apparent viscosity depends on the shear rate. Shear rate decreases with the distance from the impeller. It may fall to zero in stagnant zones (Gabelle *et al*., 2011).

Metzner and Otto (1957) believed that the fluid motion near the impeller could be explained by averaged shear rate, γ^{o}_{ave}, which is linearly related to the rotational speed of the impeller as in equation (1.9):

$$\gamma^{\circ} = k_s N \qquad (1.9)$$

The constant $k_{s,}$ depends on the impeller and tank configuration. The value of k_S reported by Metzner and Otto (1957) was 13 for a disk flat-blade turbine. Skelland (1967) reported the experimental values for k_S for different kinds of impellers such as turbines, propellers, paddles, and anchors. In case of pseudoplastic fluids, for most of the impeller types, k_S was in the range of 10-13, while for anchors and helical ribbons larger values of 25-30 was reported (Bakker and Gates, 1995).

1.5 *Impeller Type*

The selection of a suitable impeller is a critical design parameter for mixing processes utilized in chemical industries (Tahvildarian, 2010).

Mixing is used in the process industries to achieve different objectives such as blending miscible liquids in reactors, dispersing of gases or immiscible liquids into a liquid phase, and suspension of solids. Impellers related to the generated flow are classified into three groups of axial-flow, radial-flow, and close-clearance impellers.

Axial-flow impellers such as marine propellers and hydrofoil impellers discharge flow along the axis of the impeller as shown in Figure 1.3a (Oldshue, 1983). These types of

impellers are used for blending, solid- liquid suspension, and heat transfer (Paul *et al.*, 2004).

Radial-flow impellers such as disk turbines (Rushton) and hollow blade turbines (Scaba) release fluid to the wall of the tank in radial direction as shown in Figure 1.3b (Oldshue, 1983). Radial flow impellers exert shear stresses to the fluid to remove the boundary layer between various phases such as the mixing of immiscible fluids (Thring and Edwards, 1990).

Close-clearance impellers such as anchors, helical ribbons, and helical screws are used in high viscosity applications (Chhabra and Richardson, 2008). Patel *et al*. (2012) suggested that the rapidly emerging Maxblend impeller is more efficient than conventional close-clearance impellers for mixing of Newtonian and non-Newtonian fluids. Fradette *et al*. (2007) conducted some experiments with viscous Newtonian and shear-thinning fluids and proved that the Maxblend impeller provided efficient mixing with lower power consumption.

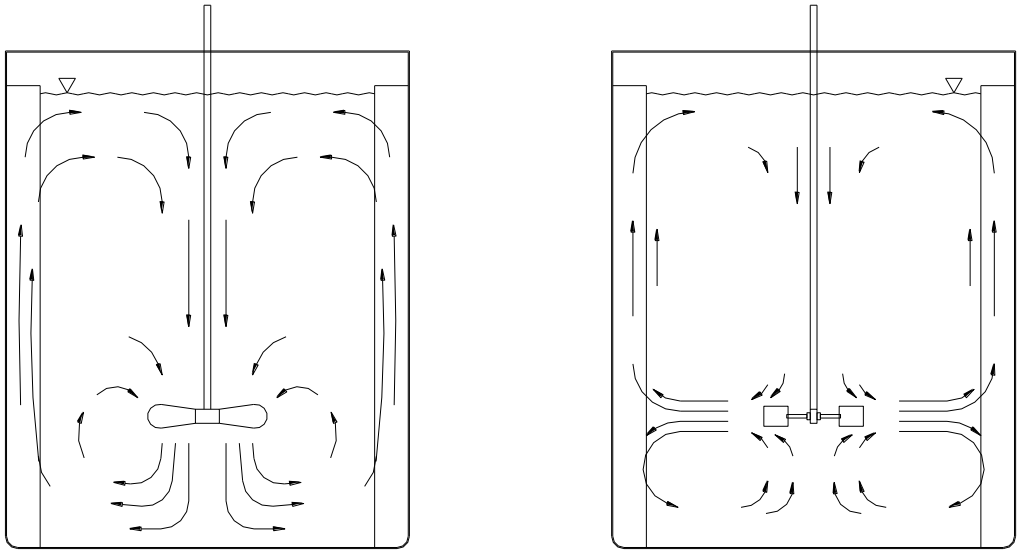

(a) **(b)**

Figure 1.3. Flow patterns in a baffled tank, generated by: (a) axial-flow impeller, and (b) radial-flow impeller.

1.5.1 Impeller Clearance

The distance between the bottom of the tank and the impeller is called clearance.

A large clearance creates a huge vortex, which results in air entrainment into the system and also causes the splash of fluid around (Paul *et al*., 2004). When an impeller is placed very close to the bottom of the vessel, the axial-flow pattern created with the downward pumping impeller is similar to the radial-flow pattern. In this situation, the bottom of the vessel becomes clear from the suspension of the particles and it leads to the reduction of the level of homogeneity in whole vessel.

1.5.2 Impeller Diameter

Impeller to tank diameter ratio (D/T) is a significant ratio in mixing tank design. Normally this ratio is selected inside a range of 0.16-0.98 (McCabe, 2005).

The diameter of the impellers which produce bulk motion such as helical ribbons, screws, and anchors should be close to the tank diameter (Tatterson, 1991).

1.6 *Fiber Suspension Mixing*

Mixing is a process which increases the degree of homogeneity and the rate of mass transfer (Paul *et al*., 2004; Bhole and Bennington, 2010). To optimize the fiber suspension mixing process, many design parameters such as the type of impeller, impeller clearance, impeller diameter, impeller speed, fiber concentration and fiber size must be considered **(**Samaniuk *et al*., 2011**).**

Hui *et al*. (2009) used a side-entering Maxflo impeller to measure the cavern size of several pulp fiber suspensions (hardwood and soft wood pulp) with suspension mass concentration from C_m = 1 % to 5 % .

Bhole and Bennington (2010) explored the performance of four axial-flow impellers (Maxflo, marine propeller, focused flow (FF), and A-312 impellers) in the mixing of hardwood bleached kraft pulp suspensions with mass concentration of 3 %. They reported that the Maxflo impeller showed better performance compared to the other three impellers.

Pimenova and Hanley (2003) measured the viscosities of corn stover using a helical ribbon impeller viscometer. Corn stover suspensions of 5, 10, 20, and 30 wt% were used in their experiments. The viscosities of the corn stover suspensions were determined for concentrations up to 30 wt%. The helical impeller method was ineffective at corn stover concentrations more than 30 wt%.

Two impellers, Rushton and helical, were utilized by Zhang *et al.* (2010) for the simultaneous saccharification and fermentation process (SSF) under a high solids loading of pre-treated corn straw. The pre-treated corn straw contained approximately 40.0 % dry solids matter (DM), and was ground in a juice blender. The results showed that the feeding time of pre-treated corn straw using the helical impeller was at least 2 hours shorter than that using the Rushton impeller. Thus, the shorter feeding time indicated that the mixing using the helical impeller was better than that using the Rushton impeller.

1.6.1 Effect of Fiber Size

The size of fiber has a prominent effect on the mixing performance. Samaniuk *et al*. (2011) measured the rheological properties of concentrated lignocellulose biomass, corn stover. They observed that the yield stress increased with the fibre length. Chaussy *et al*. (2011) examined the rheological behavior of cellulose fiber suspensions; they also observed that the suspension viscosity increased with the fiber length. Viamajala *et al*. (2009) assessed the rheology of acid hydrolyzed corn stover and reported that the yield stress decreased with a decrease in fiber size. Bashir (2008) measured the rheological

properties of wheat straw slurries at different concentrations. Based on his results, the yield stress increased with the size of the wheat straw fibers. Dasari and Berson (2007) examined the rheology of the corn stover and observed that with increasing fiber size, the yield stress increased.

1.6.2 Effect of Fiber Concentration

The literature review showed that the fiber concentration has a significant effect on the rheology of fibrous suspensions. Chaussy *et al*. (2011) examined the rheological behavior of fiber suspensions and reported that the suspension viscosity increased with the fiber concentration. Derakhshandeh *et al*. (2010b) studied the flow behavior of pulp suspensions as a function of the fiber concentration and found that by increasing the fiber mass concentration, the apparent yield stress and the consistency index in the Herschel Bulkley rheological model (K_s) increased.

Bashir (2008) measured the rheological properties of the wheat straw slurry at different concentrations and showed that the yield stress of the slurry increased with the fiber concentration. Pimenova and Hanley (2003 and 2004) measured the rheological properties of the corn stover suspensions at different concentrations. The viscosity and the yield stress of the suspension increased as the fiber concentration increased.

1.7 *Cavern*

The formation of cavern around the impeller is a characteristic of the mixing of viscoplastic fluids with yield stress such as pulp suspensions, polymers, and ceramic pastes. This class of fluids has a relatively high apparent viscosity at low shear rates. Therefore, the region around the impeller has intensive motion while elsewhere in the mixing tank is almost stagnant (Wichterle and Wein, 1975). The presence of the stagnant zones in non-Newtonian fluids are harmful to the mixing process since it leads to poor heat and mass transfer (Amanullah, 1997). Therefore, it is important to determine the cavern size and shape in these mixing operations (Adams and Barigou, 2007).

Several techniques have been used and reported in the literature for the assessment of cavern size and shape. The most significant techniques are laser Doppler anemometry (LDA), hot-wire anemometry (HWA), ultrasonic Doppler velocimetry (UDV), positron emission particle tracking (PEPT), electrical resistance tomography (ERT) and numerical techniques such as computational fluid dynamics (CFD).

1.7.1 Laser Doppler Anemometry (LDA)

This technique was first developed by Yeh and Cummins in 1964. LDA is used for measuring velocity in a non-intrusive manner by using seeded particles conveyed by a fluid flow (Drain, 1980). This is based on the measurement of laser light scattered by particles that pass through a pattern of light and dark surface. LDA measures the velocity at one point or in a very small volume, which is formed by the cross section from two-laser beams (Chaouki *et al*., 1997). Laser Doppler anemometry has been used to characterize the flow structure in stirred vessels since late 1970s (Durst *et al*., 1976;

Drain, 1980). The earlier works on caverns, using LDA, had considerable practical value to industry (Etchells *et al*., 1987; Jaworski *et al*. 1993). However, some of the fundamental concepts and the definition of the cavern boundary based on LDA measurements (Hirata *et al*., 1991) require reconsideration. The spatial and temporal resolution for this technique is very high and it can cover a huge range of flow velocities (magnitude and direction). Hirata *et al*. (1994) measured the cavern size using LDA in a shear-thinning plastic fluid agitated by the Rushton turbine. They observed the cavern shape as a circular cylinder.

1.7.2 Ultrasonic Doppler Velocimetry (UDV)

Ultrasonic Doppler Velocimetry (UDV) is a non-invasive fluid flow measurement technique, which has been used for the measurement of fluid velocity profiles (Williams, 1986; and McClements *et al*., 1990). Pulsed ultrasound echography and detection of the instantaneous Doppler shift frequency are applied in UDV to measure fluid velocity (Takeda, 1991). This technique gives an exact determination of the flow curves of complex fluids such as pulp suspensions (Derakhshandeh *et al*., 2010).

Ein-Mozaffari *et al*. (2007) examined the ability of UDV to measure the cavern size in the mixing of pulp suspensions in a rectangular tank equipped with a Maxflo impeller. Hui *et al*. (2009) also used UDV to determine the cavern dimensions in the mixing of pulp suspensions in a cylindrical tank. The UDV probes were placed at various locations around the vessel periphery to locate the points at which the suspension velocity approached zero. In this method, the data collection and analysis are time consuming compared to ERT technique.

1.7.3 Positron Emission Particle Tracking (PEPT)

Positron emission particle tracking (PEPT) is a relatively new technique allowing the quantitative study of flow phenomena in three dimensions in opaque systems that could not be studied by optical methods such as laser Doppler anemometry (LDA). Chiti *et al*. (2011) showed that the PEPT technique could be used to obtain accurate velocity data throughout the entire complex three-dimensional turbulent flow field in an agitated baffled vessel. The PEPT technique was successfully employed to visualize the cavern formed during the mixing of a slurry using a 250 μm neutral density tracer (Adams *et al*., 2008).

1.7.4 X-Ray Technique

The X-ray technique is utilized to visualize the flow patterns in the mixing of opaque fluids. Elson and Cheesman (1986) used the X-ray technique to study the flow patterns and cavern size during the mixing of opaque fluids exhibiting yield stress. Absorption of what happens when only a fraction of the radiation passes through an absorber (a heavy metal tracer). Therefore, a number of photons are lost in the absorption process. In order to use X-ray, an absorber should be added to the mixing tank. Elson (1986) measured dimensions of the cavern created around a disc turbine impeller in the mixing of xanthan gum solutions and characterized the shape of the cavern using a right circular cylinder.

1.7.5 Electrical Resistance Tomography (ERT)

ERT is a non-invasive imaging technique that measures the distribution of conductivity within a region of interest (Mann *et al*., 1997). This technique has been used in several studies, such as the formation of cavern in the mixing of pseudoplastic fluids (Pakzad *et al*., 2008), investigation of mixing processes (Kim *et al*., 2006), solid-liquid filtration processes (Vlaev *et al*., 2000), multiphase processes like solid-liquid (Lucas *et al*., 1999; Recard *et al*., 2005), gas-liquid (Wang *et al*., 2000), and liquid-liquid (Kaminoyama *et al*., 2007).

1.7.6 Numerical Model

1.7.6.1 Computational Fluid Dynamics (CFD)

Computational fluid dynamics (CFD) is a technique to analyze a system involving fluid flow and other related phenomena through mathematical modeling based on computer programs (Hosseini *et al*., 2009). The CFD provides useful information regarding the impeller pumping capacity, flow pattern, and the formation of cavern around the impeller. Pakzad *et al*. (2008) employed CFD technique to analyze the formation of cavern around a Scaba impeller rotating in a yield-pseudoplastic fluid. The CFD results were in good agreement with the experimental data determined using the tomography technique.

Adams and Barigou (2006) studied the formation of caverns in a yield-stress fluid of the Herschel–Bulkley type and pseudo-cavern in a shear-thinning power-law fluid, both in the laminar and transitional flow regimes using a CFD model. They determined that CFD

predictions of cavern size agreed very well with experimental measurements at low Reynolds numbers.

1.8 *Cavern Mathematical Models*

Several mathematical models were developed over the years to predict the cavern size as a function of mixing conditions and fluid properties, such as spherical (Solomon *et al*., 1981), cylindrical (Elson *et al*., 1986 and 1988; Hirata and Aoshima, 1994 and 1996) and toroidal (Amanullah *et al*., 1998; Wilkens *et al*., 2005). In all cases, the models were developed for the isolated cavern that does not make contact with the vessel walls (Hui *et al*., 2009).

For the models mentioned above, researchers considered different flow regimes inside the cavern as well as different forces (tangential and axial), and used different rheological models such as Herschel-Bulkley and Bingham plastic.

1.8.1 The Spherical Model

Solomon *et al*. (1981) developed a theoretical model for a spherical cavern. The basis of this model is that the shear stress equals the fluid yield stress at the cavern boundary. The model assumes that the predominant motion of the fluid within the cavern is tangential and is equivalent to the flow in an unbaffled vessel. The equation given by Solomon *et al.* (1981) is:

$$\left(\frac{D_c}{D}\right)^3 = \left(\frac{4P_0}{\pi^3}\right)\left(\frac{N^2 D^2 \rho}{\tau_y}\right) \tag{1.10}$$

when $D \leq D_C \leq T$ (Tank diameter), where D_C is the cavern diameter, D is the impeller diameter, P_o is the power number, N is the impeller speed, ρ is fluid density and τ_y is fluid yield stress. The term $N^2D^2\rho/\tau_y$ on the right hand side of the equation (1.10) is called the yield stress Reynolds number, and is usually shown as Re_y (Etchells *et al*., 1987).

1.8.2 The Cylindrical Model (Elson's Model)

The cylindrical model was proposed by Elson *et al.* (1986 and 1988). The model indicates that the cubed cavern diameter ratio $(Dc/D)^3$ is proportional to the product of the power number and the "yield Reynolds number" as shown by equation (1.11):

$$\left(\frac{D_c}{D}\right)^3 = \left[\frac{1}{\left(H_c/D_c + 1/3\right)\pi^2}\right]\left(\frac{N^2D^2\rho}{\tau_y}\right)P_0 \qquad (1.11)$$

where in this equation, D_c/D is dimensionless cavern diameter, $N^2D^2\rho/\tau_y$ is the yield stress Reynolds number, and H_c is the cavern height, and P_0 is the power number.

Amanullah *et al*. (1998) reported that both spherical and cylindrical models predicted the cavern diameter equally well. However, they believed that the cylindrical model was a better representation of the cavern shape.

1.8.3 The Torus-shaped Model

A mathematical (axial force) model was created by Amanullah *et al*. (1998). This model assumes entire momentum passed on by the impeller as the sum of both tangential and axial shear components, transmitted to the cavern boundary by the pumping action of the impeller. The equation given by Amanullah *et al*. (1998) is as follows:

$$\left(\frac{D_c}{D}\right)^2 = \frac{1}{\pi}\sqrt{N_f + \left(\frac{4P_0}{3\pi}\right)^2}\left(\frac{N^2D^2\rho}{\tau_y}\right) \tag{1.12}$$

where $N_f = F_a /PN^2D^4$ is the dimensionless axial force number, F_a is the axial force imparted by the impeller and P is the power. This model can also be applied to the caverns generated by radial flow impellers if $N_f = 0$, as follows (Bhole and Bennington, 2010):

$$\left(\frac{D_c}{D}\right)^2 = \frac{1}{3}\left(\frac{4P_0}{\pi^2}\right)\left(\frac{N^2D^2\rho}{\tau_y}\right) \tag{1.13}$$

In the literature, there seems to be no study on the cavern evaluation of wheat straw suspensions. The recent and rapid development of non-intrusive ERT seems to provide an efficient tool for the analysis and control of mixing processes, especially in the case of non-Newtonian fluids (either opaque or transparent). Electrical resistance tomography (ERT), which is an emerging technology, can be the best alternative to measure the cavern size and analyze fluid flow in 2D and 3D.

1.9 *Research Objectives*

From the literature review, one can say that the information regarding mixing of wheat straw slurry is still inadequate. This study will try to employ ERT to study the mixing of this pseudoplastic fluid with axial impellers (A100, A200, and A310). The main contributions of this work are:

- To employ Electrical Resistance Tomography (ERT) to predict the cavern dimensions of the cavern formed around the impellers
- To study the effects of wheat straw slurry concentration on the cavern size
- To study the effects of wheat straw fiber size on the cavern size
- To understand the flow field generated by the A100, A200, and A310 impellers.

CHAPTER 2

Electrical Resistance Tomography (ERT)

As described in chapter 1, many techniques are available to measure the cavern size. However, those techniques have their own restrictions such as limitation in working with opaque fluids and changing the local flow field. To solve these issues, a non-intrusive technique called electrical resistance tomography (ERT) can be utilized to measure the cavern size.

ERT is a measurement technique which is used in several studies such as the investigation of mixing processes (Kim *et al*., 2006), examination of solid-liquid filtration processes (Vlaev *et al*., 2000), and also observation of multiphase processes such as solid-liquid (Lucas *et al*., 1999; Recard *et al.*, 2005), gas-liquid (Wang *et al*., 2000) and liquid-liquid (Kaminoyama *et al*., 2007). This technique not only measures the mixing time but also allows observation of the dynamic of mixing for both transparent and opaque fluids. The ability of ERT to work in opaque fluids makes this technique very attractive from an industrial perspective since most of the fluids encountered in industrial mixing processes are opaque fluids such as pulp suspensions, ketchup, mayonnaise, paints, cement, pigment slurries, certain polymer and biopolymer solutions, and wastewater sludge (Ihejirika and Ein-Mozaffari, 2007).

2.1 *Principal elements of the ERT system*

The objective in electrical tomography technique is to measure electrical signals sent from sensing electrodes and to reconstruct the conducting properties of the fluid inside of the mixing vessel (William *et al*., 1993; Holden *et al*., 1998; and Tahvildarian *et al*., 2011).

The goal of ERT system is to obtain the resistance distribution in the domain of interest. The ERT system consists of three main components: the sensors, the data acquisition system (DAS) and the image reconstruction system.

2.1.1 Sensing System

Electrodes are the heart of the ERT system. They must be in continuous contact with the fluid inside the vessel. The position of the electrodes is important since the reconstruction algorithm is based on the electrodes being located at exactly defined intervals in order to outline the maximum amount of information from inside of the vessel (Kaminoyama *et al.*, 2007). The size of the electrodes is another important factor in measuring the electric field distribution (Mann *et al*., 1996).

In this method, multiple electrodes are located around the wall of the mixing vessel (Zhao *et al.*, 2008; Pakzad *et al.*, 2008). An electrical current is applied to two adjacent electrodes and the voltages are measured between the other adjacent electrode pairs (Williams and Beck, 1995). To receive accurate measurement, the electrodes must be more conductive than the fluid (Tahvildarian *et al*., 2011). The electrodes, which are

located around the boundary of the vessel, make the electrical contact with the fluid inside the vessel and are connected to the data acquisition system (DAS) by co-axial cables to reduce electromagnetic noise and interference (Dickin and Wang, 1996).

Electrodes can be fabricated from gold, platinum, stainless steel, brass, or silver (Paulson *et al*., 1992).

2.1.2 Data Acquisition System (DAS)

A data acquisition system (DAS) is connected to the electrodes and communicates with the host image reconstruction computer.

DAS is responsible for signal measurement, filter and control, demodulation, multiplexer control, waveform generation, synchronization, and power supply (Holden *et al*., 1998). It is necessary to select the scheme that has a good distinguishability and high sensitivity to conductivity changes in the fluid. Figure 2.1 shows a schematic diagram of the ERT data acquisition system (DAS), made of six functional parts.

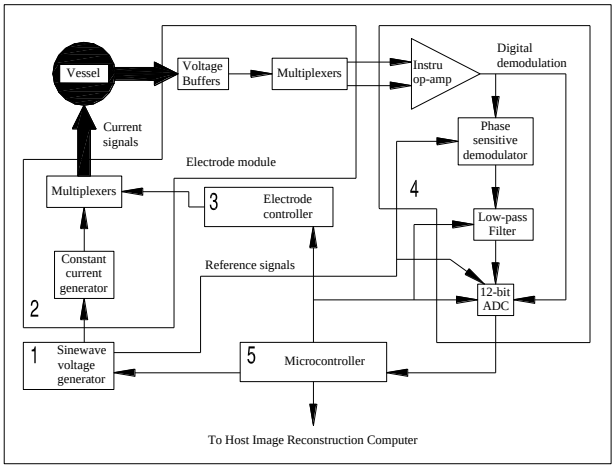

Figure 2.1. Components of a typical data-acquisition system (Holden *et al*., 1998)

The digital “stir-case” generators are used to generate staircase wave. A high-speed digital to analogue converter (DAC) converts the digital pattern to analogue and subsequently filters to reduce unwanted harmonics. The major part of DAS is voltage generator. The output of this part is a sine wave voltage that is sent to a voltage-to-current convertor. Multiplexers (MUX) are necessary to share the current source and voltage measurement stages between any numbers of electrodes (Beck *et al.*, 1993).

The data acquisition system is responsible to perform the desired measurement protocol. As can be seen in Figure 2.2, an adjacent measurement protocol is used to apply an AC current between two adjacent electrodes and to measure the voltage between all other pairs of adjacent electrodes. The AC current is then applied to the next pair of electrodes and the voltage is measured for all other electrode pairs (Barber *et al.*, 1983).

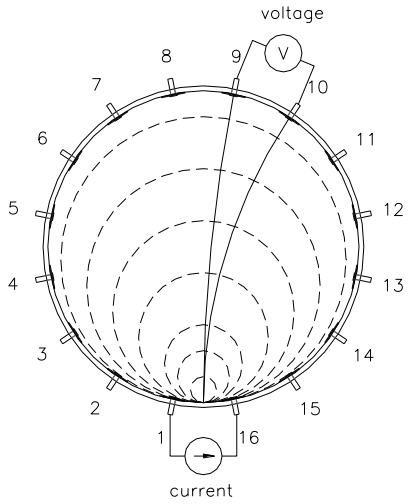

Figure 2.2. Data collection strategy; adjacent measurement strategy (Pakzad, 2007)

2.1.3 Data Collection Strategies

There are four main strategies to examine conductivity distribution in a tank and to gain maximum information, as follow:

- Adjacent strategy
- Opposite strategy
- Diagonal strategy
- Conducting boundary strategy

2.1.3.1. The Adjacent Strategy

This strategy is used for sensors with insulating boundaries. In this strategy, current is applied through two neighbouring electrodes and the voltage differences are measured using all other pairs of neighbouring electrodes. To repeat this process, the current is applied to all other possible pairs of neighbouring electrodes. In this strategy, the total number of independent measurements (M) achieved is given by equation (2.1):

$$M = \frac{N(N-3)}{2} \tag{2.1}$$

where N is number of electrodes.

This strategy entails minimal hardware to implement and image reconstruction. It is very delicate to measure error and noise, based on the non-uniformity of the current distribution and the low current density at the center of the vessel (Mann *et al*., 1997; Kaminoyama, 2005).

2.1.3.2. The Opposite Strategy

In this strategy, current is applied through diametrically opposed electrodes. The voltage reference is that to the electrode adjacent to the current-injecting electrode. The voltages are measured with respect to the reference, at all electrodes except the current-injecting ones. The whole process is repeated in the clockwise direction until all independent measurements have been made. In this case, the total number of independent measurements *M* is calculated as follows (Viergever and Todd-Pokropek, 1988):

$$M = \frac{N}{4}\left(\frac{3N}{2} - 1\right) \tag{2.2}$$

Compared to the adjacent strategy, the opposite strategy is less sensitive to conductivity changes at the boundary because most of the current runs through the central part of the region (Hua *et al*., 1993). The opposite strategy has less image resolution than the adjacent strategy, due to the reduced number of independent current projections (Abdullah, 1993).

2.1.3.3. The Diagonal Strategy

In this strategy, a current is applied between electrodes separated by large dimensions. Electrodes 1 and 2 are fixed as the current reference and the voltage reference, respectively. Then, the current is applied to electrodes 3, 5, 7, etc., and the voltage is measured from electrodes to the left of electrode number 2. Then the current reference and voltage reference are changed to electrode 4 and electrode 3, respectively. Sending

current through electrodes 2, 6, 8, etc., the voltage is measured on all other electrodes except the current-injecting ones. This strategy, compared with the adjacent strategy, has a good sensitivity over the entire vessel and gives better quality (Hua *et al.,* 1993).

2.1.3.4. The Conducting Boundary Strategy

In this strategy, both current and voltage are used between two electrodes. The main benefit of this strategy is its low common-mode voltage component. The large surface area of the conducting boundary is used as the current sink to reduce the common-mode voltage across the electrodes doing the measurement (Gisser *et al*., 1987).

The common-mode voltage for conducting boundary strategy is greatly reduced compared with that of the adjacent strategy (Dickin and Wang, 1996).

2.1.3 Image Reconstruction System

The adjacent strategy provides 104 individual voltage measurements for each plane with 16 electrodes according to the equation n_e (n_e-3)/2, where n_e is the number of electrodes per plane. Eventually, the DAS communicates the quantitative data to the host image reconstruction computer, where data are processed using a suitable image reconstruction algorithm. An image reconstruction algorithm is applied to determine the interior distribution of the resistance in the process vessel after gaining the measurements from a set of electrodes sitting on the border of a vessel (Pinheiro *et al*., 1999; Mann *et al.,* 1996). There are two types of algorithms: non-iterative and iterative. A non-iterative

image reconstruction algorithm (Linear Back Projection-LBP) is used to convert a voltage measurement to conductivity values of each plane (Barber and Brown, 1984). The linear back projection algorithm, compared to an iterative image reconstruction algorithm, has a low computational requirement (Wang, 2002). The iterative algorithm has high computational requirement and is too slow for real-time image reconstruction compared to the non-iterative algorithm (Madupu et al., 2005).

The P2000 system (Industrial Tomography Systems-ITS, Manchester, UK), used in this study, comes with a qualitative, non-iterative algorithm on linear back-projection.

CHAPTER 3

EXPERIMENTAL SETUP AND PROCEDURE

3.1 *Material and Methods*

In this study, we assessed the mixing of aqueous wheat straw slurries of 5 wt%, 7 wt%, and 10 wt% concentration. Wheat straw was generously donated by the Ontario Schomberg farm. In order to study the effect of the fiber length, two sizes ($\leq$ 2 mm and (8 mm $\pm$ 0.014 mm) of the wheat straw were prepared. The Cutting Mill SM 100 (Master Craft, United States) grinded the wheat straw to $\leq$ 2 mm. Scissors were used to cut the wheat straw to 8 mm. During the experiments, the tank was filled with tap water to a height (H) of 400 mm.

For each test, the required amount of the wheat straw was loaded into the mixing vessel and the tap water was added to reach the desired slurry height (400 mm) inside the tank.

In this study, experiments were conducted using three impellers at many impeller speeds, and for two fiber sizes. Table 3.1 summarizes the operating conditions for all experiments conducted in this study.

Table 3.1. Experimental conditions[1]

Impeller Speed N (rpm)	30 - 120 rpm
Impeller Type	A100, A200, and A310
Fiber Size	≤ 2 mm and 8 mm
Slurry Concentration	5 wt%, 7 wt%, 10 wt%

3.2 *Experimental Setup*

Figure 3.1 shows the schematic diagram of the experimental setup utilized in this study. Mixing system used in this study consists of a flat-bottomed cylindrical tank with a diameter of 400 mm and a height of 600 mm. The tank was equipped with two equally spaced baffles with a width of 30 mm.

The slurry height (H) in the tank was 400 mm. The tank consisted of four tomography sensor planes. The planes were 86 mm apart from each other with the bottom plane 74 mm from the bottom of the tank. The planes were numbered from top ($P1$) to bottom ($P4$). Each plane had 16 stainless steel electrodes, which were located equidistantly on the periphery of the vessel. The height, width, and thickness of the electrodes were 20 mm, 30 mm, and 1 mm, respectively. Each electrode was connected to the electrical resistance tomography system (Industrial Tomography Systems, Manchester, UK), which was connected to a computer for the image reconstruction.

[1] The sample of detailed table and explanation regarding the experiments are placed in Appendix A.

The mixing tank was equipped with a top-entering impeller driven by a 2-hp motor. The impeller rotational speed was varied using a variable frequency drive. The impeller torque and speed were measured using a rotary torque meter (Staiger Mohilo, Germany) and a tachometer, respectively. In this study three impellers were used (A100, A200, A310), each with a 180 mm diameter (*D*). Each impeller was located on plane *P3* with an off-bottom clearance of 160 mm.

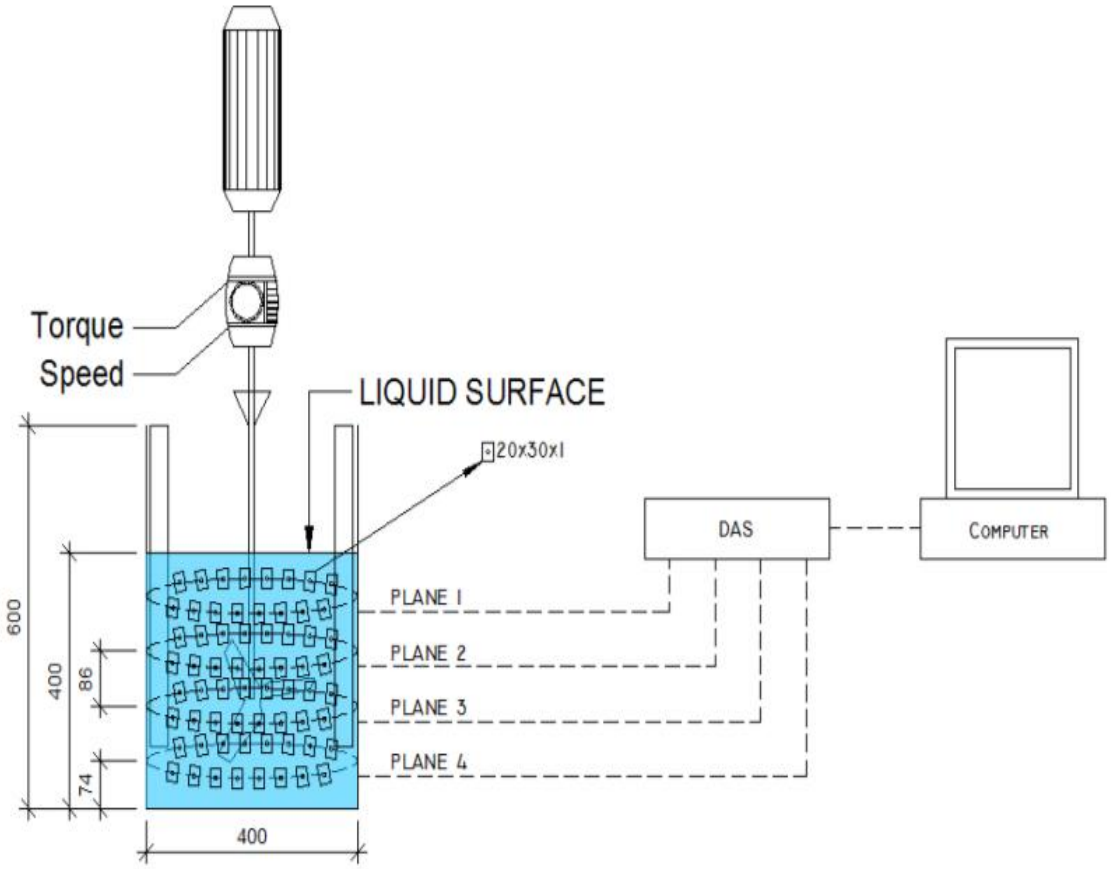

Figure 3.1. Schematic diagram of the experimental setup used in this study (all units in mm)

A100 (marine propeller) is a three rounded and twisted blade impeller with a 45° blade angle (Figure 3.2). A100 impeller produces an axial flow directed to the bottom of the vessel and has a high discharge capacity with low head.

Figure 3.2. Impeller A100 used in this study

A200 (pitched blade turbine) is a four blade impeller with a 45° blade angle (Figure 3.3). This impeller generates an axial-flow pattern. Normally this impeller is used for low to medium viscosity flow.

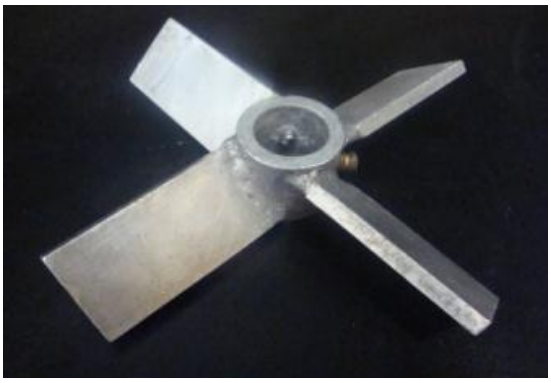

Figure 3.3. Impeller A200 used in this study

A310 is a 45° blade angle with three twisted blade impeller (Figure 3.4). The blade tip of this impeller creates a consistent velocity across the entire discharge area. This impeller is very useful for low viscosity fluids.

Figure 3.4. Impeller A310 used in this study

3.2.1 Power Measurements

The power input to the impeller (P) was obtained from torque (M) and impeller rotational speed (N) measurements using:

$$P = 2\pi NM \tag{3.1}$$

Impeller torque and speed were measured using a torque sensor (Staiger Mohilo, Germany). The bearing friction was measured by operating the system with an empty vessel. This friction torque was subtracted from all subsequent measured torques.

3.2.2 Using tomography to measure the cavern size

In this study, electrical resistance tomography (ERT) was utilized to measure the cavern size. To achieve this goal, 30 mL of 20% saline solution (as a tracer) was injected into the wheat straw slurry near the impeller blade using a plastic syringe after the mixing system reached steady-state conditions. The injection took about 2-3 s for all experiments. A conductivity meter (PC10 portable meter, Oakton Instruments, USA) was employed to take an individual conductivity measurement before each experiment run to make sure that the conductivity of the wheat straw slurries were the same for all experiments. The size of the cavern was measured after the injection once the cavern size remained unchanged. The cavern boundary was determined as a position at which the tracer concentration was zero. Each tomography test was repeated three times. The standard deviation was found to be 0.56 % for cavern dimensions.

Colors in tomograms display the dispersion of the tracer in the vessel (Fig 3.5). The dark blue color in these tomograms demonstrates low-conductivity zones, which represents lower tracer concentration. The red color in the tomograms shows the high-conductivity regions, which indicates the higher tracer concentration in those zones. At the boundary of the cavern, the concentration of the tracer was zero. This means that the conductivity of the slurry at the cavern boundary was equal to the conductivity of the slurry before the injection of the tracer.

The 2D tomogram shows that the tracer injected near the impeller blade remained within the cavern and no tracer was found in the surrounding.

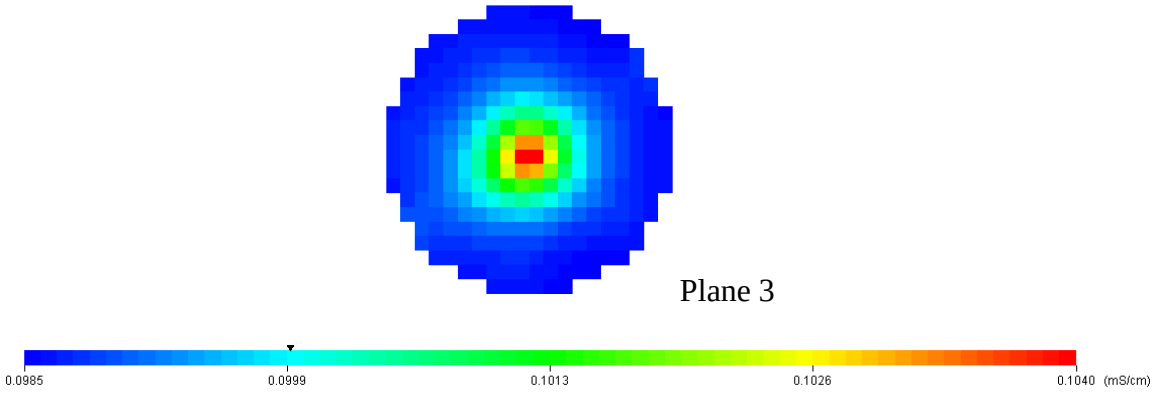

Figure 3.5. Tomogram of the cavern formation for 10 wt% wheat straw slurries (≤ 2 mm) agitated by the A100 impeller at 60 rpm

3.3 *Xanthan Gum as a Reference to Check the Accuracy of the Tomography Measurements*

In this study, an aqueous 0.5 wt% xanthan gum solution was used as a reference to check the accuracy of the ERT measurements. To prepare xanthan gum solutions, 2.5 kg of the xanthan gum powder was added slowly to water in the tank while the A310 impeller was working.

ERT was able to image the cavern formed around the impeller at 0.5 wt% xanthan gum solution once 30 ml of 10% saline solution tracer was injected near the impeller blade. Measurements of cavern were collected from the four planes of electrodes until the cavern size remained unchanged. These tomography images were then used to measure the cavern diameter (D_c) and cavern height (H_c), using 2D and 3D images respectively. Figure 3.6 shows the formation of cavern visualized using the two dimensional (2D)

tomograms generated after the injection of the saline tracer in the mixing of 0.5 wt% xanthan gum solution using A310 impeller. As shown in the figure, the impeller was located on the plane *P*3.

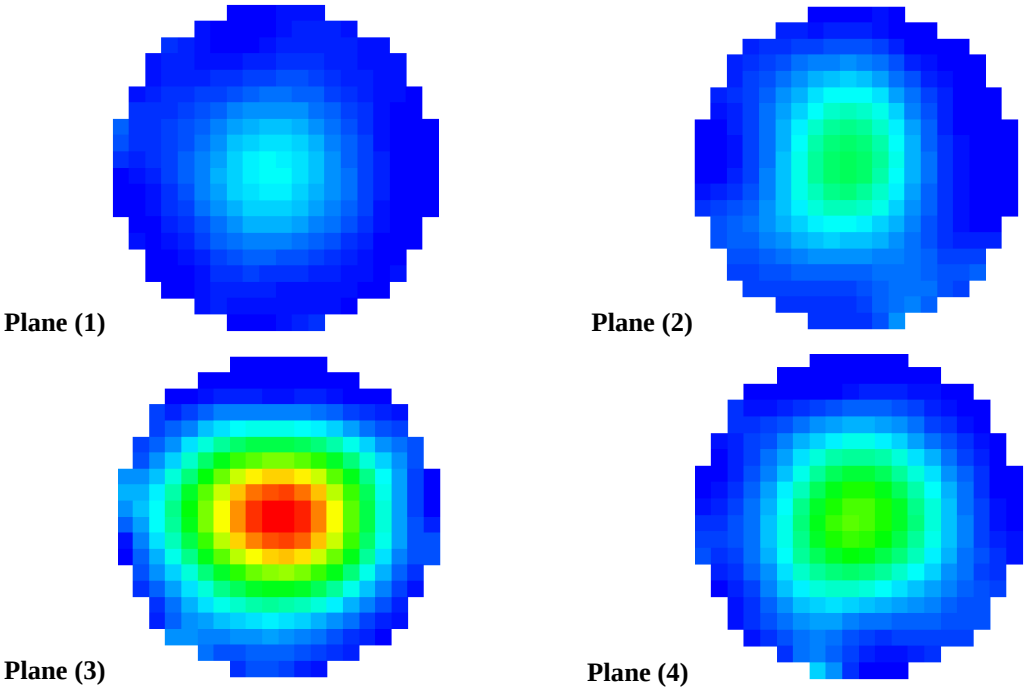

Figure 3.6. Cavern formation in agitation of 0.5 wt% xanthan gum solution at 30 rpm agitated by A310 impeller

The cavern dimensions obtained from the tomography measurements were then substituted into the cylindrical model proposed by Elson (Equation 1.11), and the yield stress for 0.5 wt% xanthan gum solution was calculated. As shown in Table 3.2, the yield stress estimated using the tomography images was in good agreement with that measured

using a Bohlin CVOR Rheometer 150 (Malvern Instruments, USA) as reported by Pakzad (2007). The relative error between the estimated values obtained from the rheometry and the tomography techniques was 0.61 %.

Table 3.2. Comparison between the yield stresses measured using ERT and rheometer

Xanthan gum yield stress (Pa) measured by Rheometer	**Xanthan gum yield Stress (Pa) measured using ERT**
1.79 (Pakzad, 2007)	1.80±0.01

CHAPTER 4

RESULTS AND DISCUSSION

In this chapter, the experimental results are presented and discussed for the impeller torque, power consumption, yield stress, and cavern formation in the mixing of wheat straw slurries as a function of the impeller type, impeller speed, slurry concentration, and fiber size.

4.1 *Torque and Power Measurements*

4.1.1 Evaluation of the Torque Sensor Precision

The impeller torque was measured using a rotary torque meter (Staiger Mohilo, Germany) as a function of the impeller rotational speed. Each test was repeated 3 times and the standard deviation for the torque measurements was calculated using the following equation:

$$\sigma = \sqrt{\frac{1}{N}\sum_{i=1}^{N}\left(M_i - \overline{M}\right)^2} \qquad (4.1)$$

where N is the number of measurements, M_i is the torque measurement for sample i and $\overline{M}$ is the mean value of the torque measurements.

Figure 4.1 shows the torque versus the impeller speed as a function of the slurry concentration for fiber ≤ 2 mm. The figure shows spread of the torque about the mean value as indicated by the error bar obtained using the standard deviation. Based on the error bars, we can see that the errors were small enough ($\sigma < 0.01$) to be acceptable.

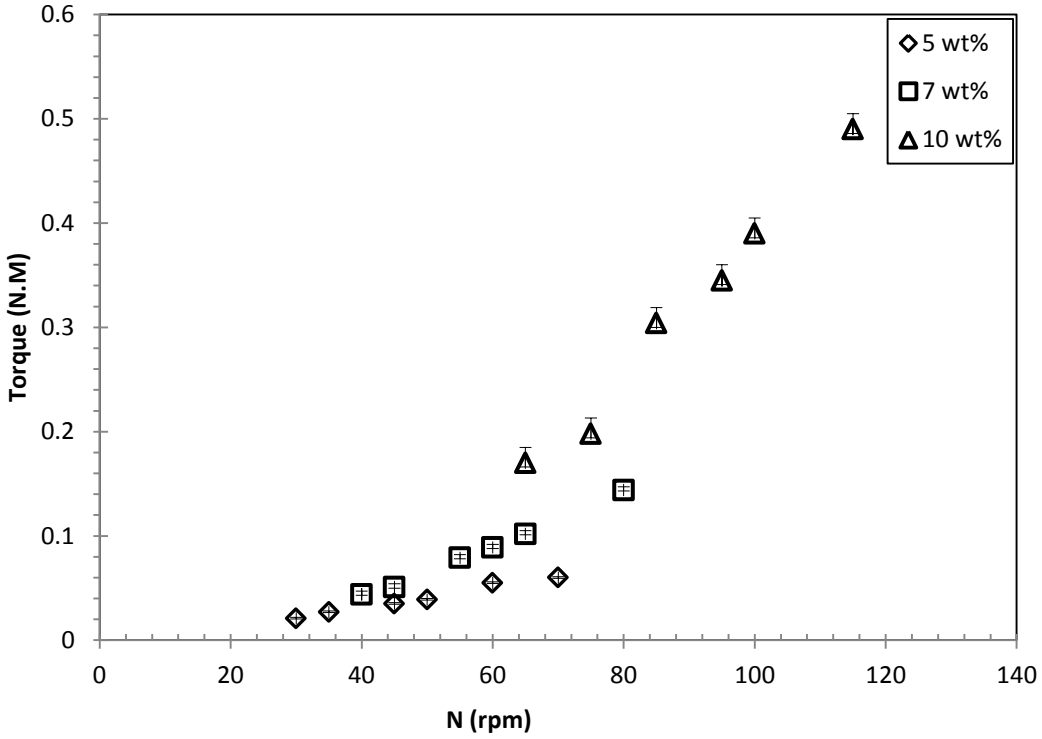

Figure 4.1. Torque versus impeller speed for 5, 7, and 10 wt% wheat straw (≤ 2 mm) agitated by A310 impeller

Figure 4.2 depicts the torque versus the impeller speed as a function of the slurry concentration for fibers of 8 mm. By increasing the fiber concentration and fiber size, the impeller torque increased. When fiber size and fiber concentration increased the strength

of the slurry networks increased as well. Therefore, the yield stress of the slurry increased and it caused an increase of the impeller torque.

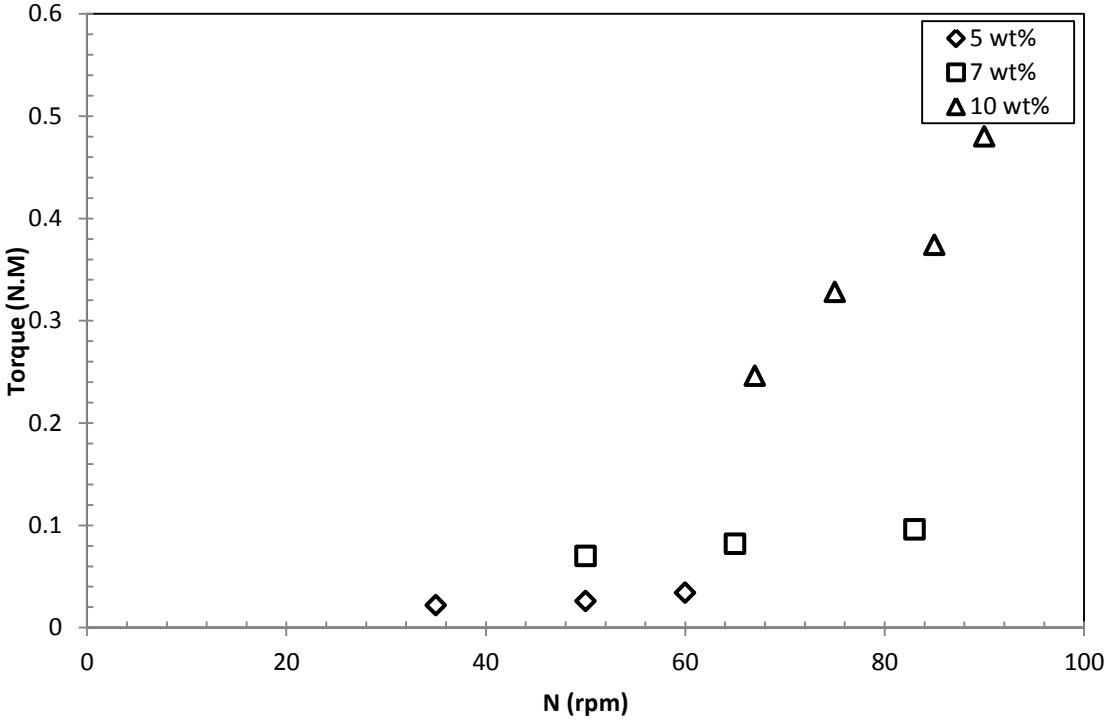

Figure 4.2. Torque versus impeller speed for 5, 7 and 10 wt% wheat straw (8 mm) agitated by A310 Impeller

As shown in Figure 4.3, for the same size and concentration of wheat straw at 80 rpm, impeller A100 shows highest torque compared to impellers A310 and A200. Impeller A200 has the lowest torque**.**

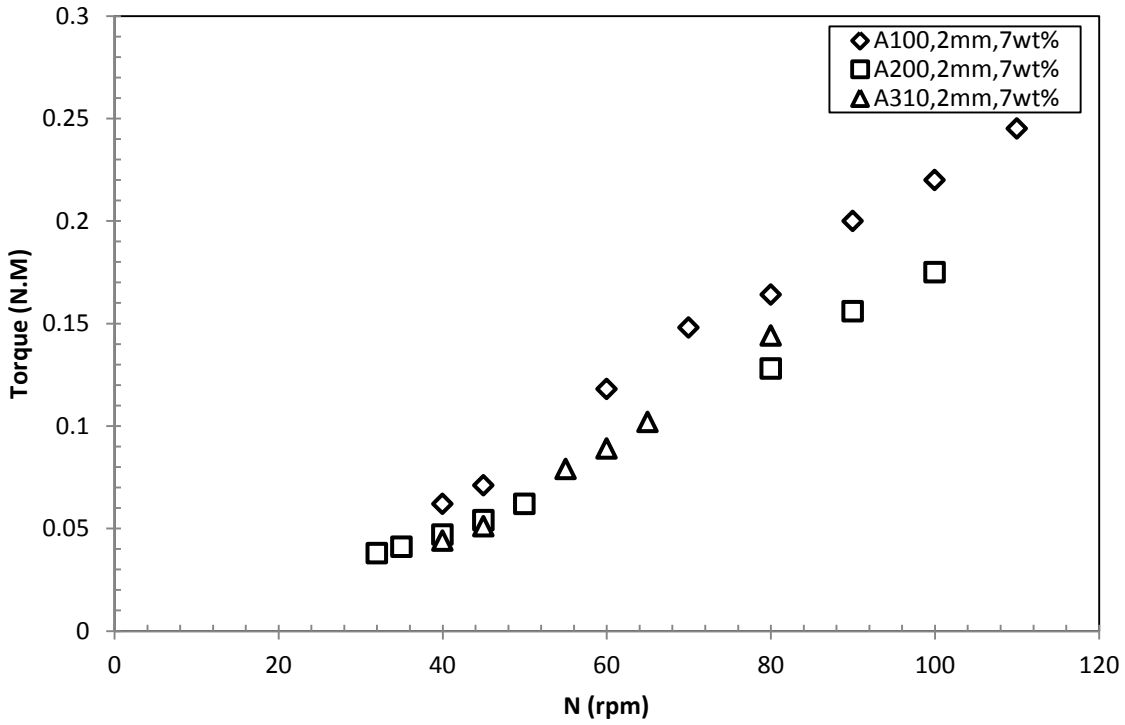

Figure 4.3. Torque versus impeller speed for 7 wt% wheat straw (≤ 2 mm) agitated by A100, A200 and A310 impellers

4.2 *Cavern Formation in Mixing Wheat Straw Slurries*

Several experimental methods have been employed to investigate the formation of cavern as discussed in literature review; each of these techniques has its own restrictions. In order to prevail over these limitations, electrical resistance tomography, which is an emerging technology, can be the best alternative to measure the cavern size and analyze fluid flow in 2D and 3D in this study.

4.2.1 Using ERT to Measure the Cavern Diameter and Height

In this study, the size of cavern formed around the impeller in the mixing of the wheat straw slurries was measured as a function of the impeller type and speed for two sizes of wheat straw fibres (≤ 2mm and 8 ± 0.014 mm) with 5, 7, and 10 wt% fiber through the tomography images.

Figure 4.4 illustrates the formation of cavern based on the conductivity distribution visualized using the two dimensional (2D) tomograms generated after the injection of the saline tracer in the mixing of 10 wt% of wheat straw slurry (≤ 2 mm) agitated by A310 impeller at 60 rpm. The 2D tomograms provided the diameter of the cavern.

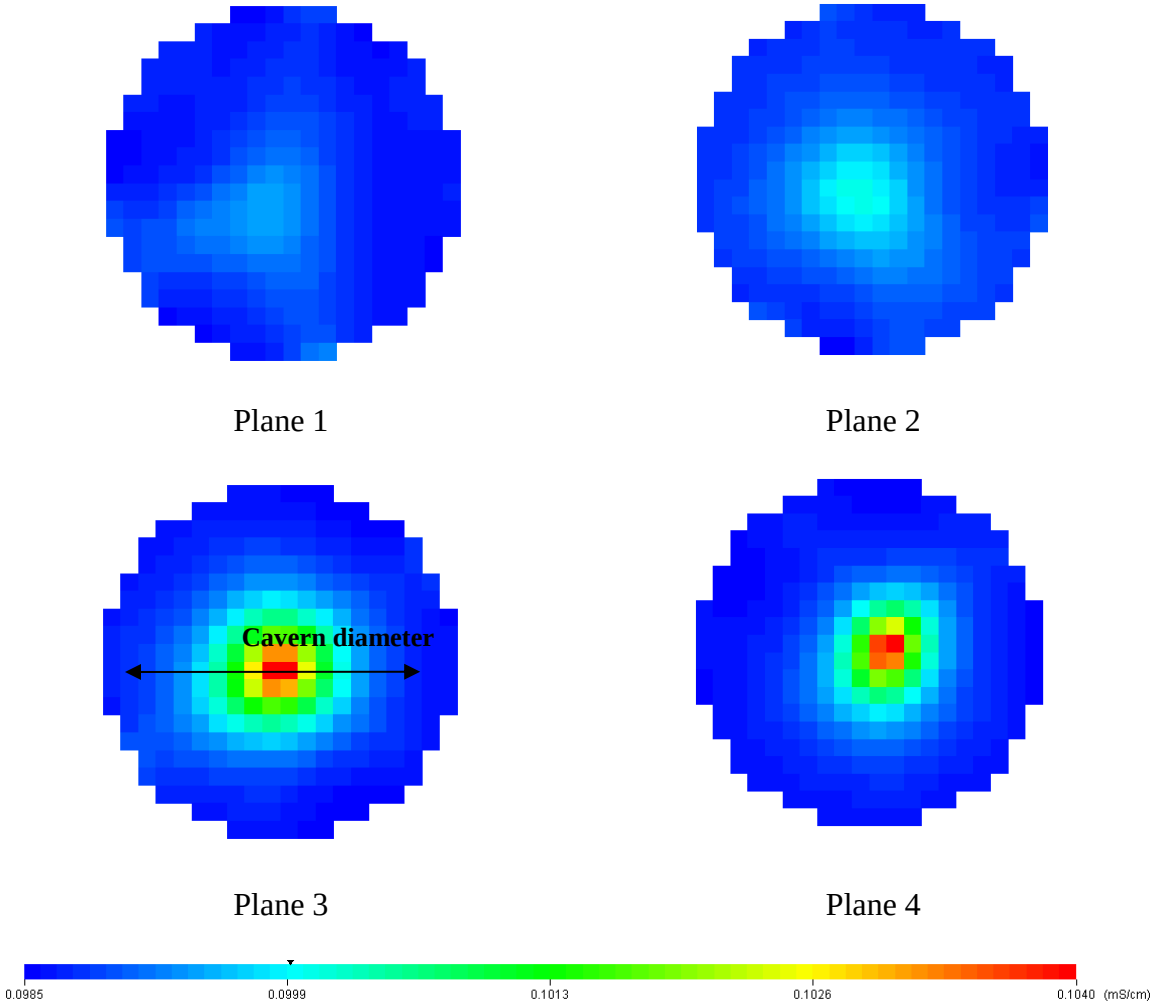

Figure 4.4. Cavern formation in 10 wt% wheat straw slurry (≤ 2 mm) agitated by A310 impeller at 60 rpm

The 3D images provided the height of the cavern. The cavern height was measured using the vertical slice images as shown in Figure 4.5.

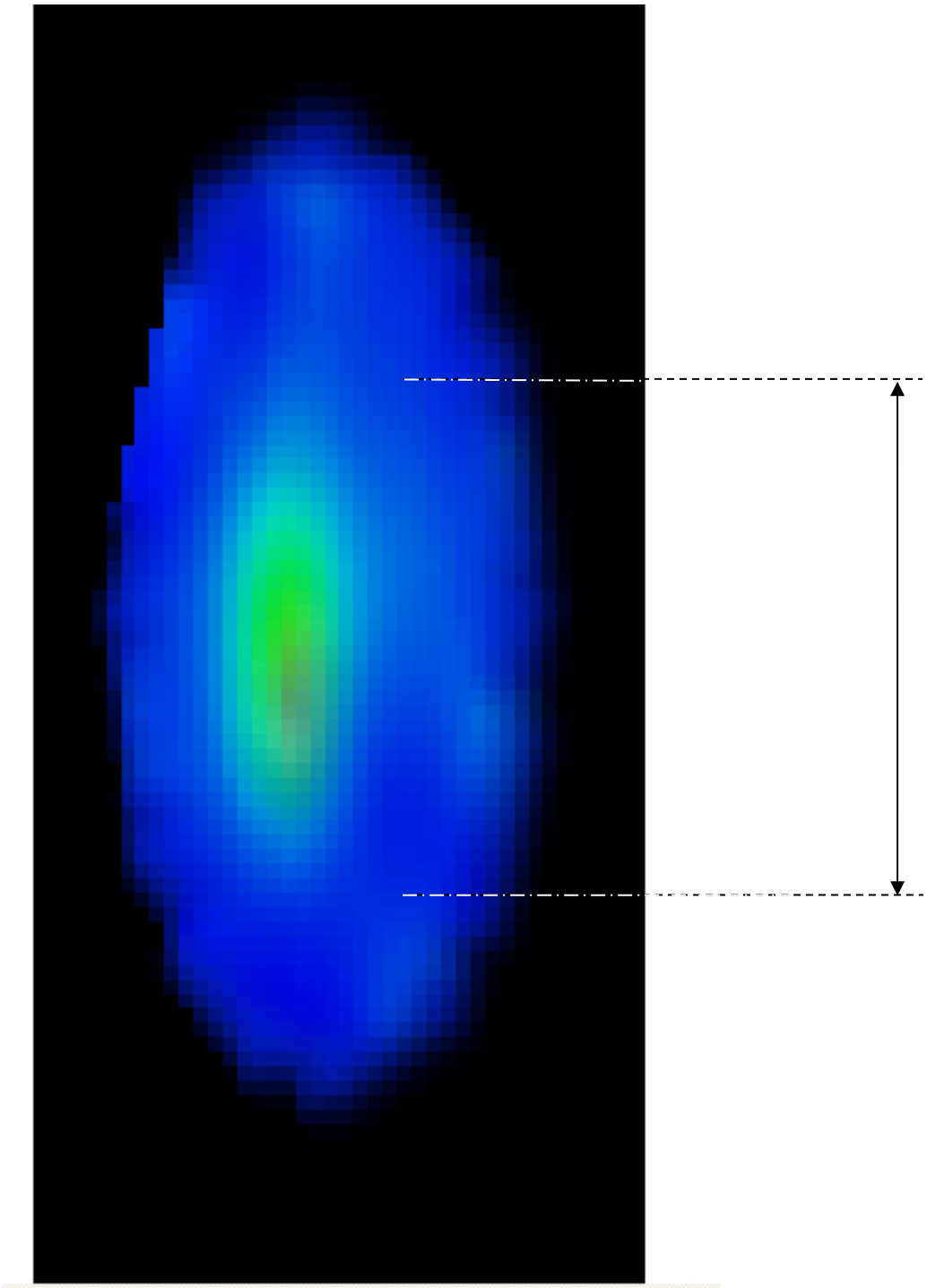

Figure 4.5. Cavern height in agitation of 10 wt% wheat straw suspension (≤ 2 mm) agitated by A310 impeller using 3D tomogram at 60 rpm.

4.2.2 Dimensionless Cavern Diameter (*Dc/D*)

Various models have been recommended in the literature (Solomon *et al*., 1981; Elson *et al*., 1986 and 1988) to estimate the dimensionless cavern diameter (*Dc/D*) versus the product of two dimensionless groups of P_o and $Re_y = \rho N^2 D^2/\tau_y$. As mentioned before, *Dc* is the cavern diameter, *D* is the impeller diameter, P_o is the impeller power number, and Re_y is the yield stress Reynolds number. According to Elson's model equation (1.11), a plot of the dimensionless cavern diameter, *Dc*/*D*, versus $P_o\, Re_y$ is a straight line with a slope of 0.33 in log-log scale. This model defines the formation of a cylindrical cavern centered upon the impeller. In the following sections, the cavern dimensions measured using tomography technique at different operating conditions were fitted to Elson's cylindrical model.

4.2.2.1 Effect of Wheat Straw Concentration on the Cavern Dimensions

Figure 4.6 shows the effect of wheat straw concentration on the cavern diameter when a wheat straw slurry of ≤ 2 mm fiber size was agitated by the A200 impeller at 70 rpm. It shows the cavern diameter of 32 cm, 28 cm and 21 cm for wheat straw concentration of 5 wt%, 7 wt%, and 10 wt% respectively.

The largest cavern diameter was measured for 5 wt% wheat straw slurries. This finding is in agreement with those reported in the literature. For instance, Pakzad *et al.* (2008) showed that by increasing the yield stress, the cavern diameter decreased. In fact, the presence of the yield stress leads to the formation of stagnant regions outside the cavern in which the shear stress falls below the slurry yield stress.

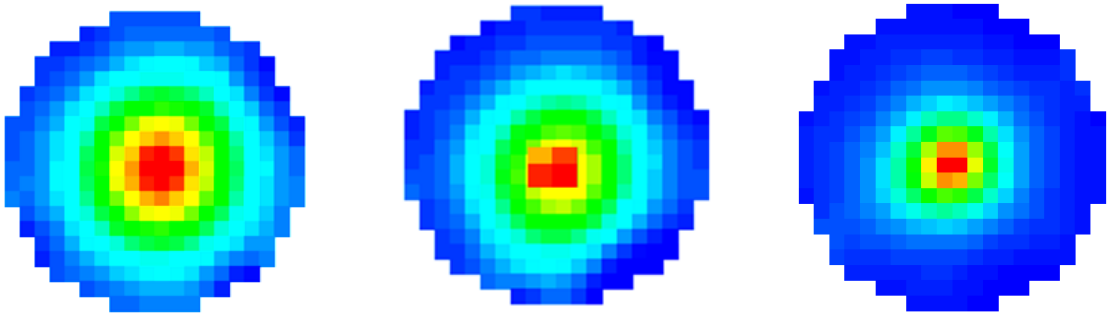

(a) 5wt% **(b)** 7wt% **(c)**10wt%

Figure 4.6. The effect of wheat straw (≤ 2 mm) concentration on the cavern diameter agitated by the A200 impeller at 70 rpm for (a) 5 wt%, (b) 7 wt% and (c) 10 wt%

Figures 4.7 to 4.9 show the dimensionless cavern diameter versus the product of P_o (power number) and $\rho N^2 D^2/\tau_y$ (Reynolds yield stress) for the three impellers used in this study for all three concentrations. The slopes of the D_c/D versus $P_o\, Re_y$ for A100, A200, and A310 impellers were 0.24, 0.26, and 0.29, respectively. These slopes are lower than that expected from Elson's model (0.33). However, our results for these three axial-flow impellers were in good agreement with those reported in the literature. For example, Patel *et al.* (2012) reported a value of 0.23 for A310 while Saeed *et al*. (2008) reported a value of 0.24 for three axial-flow impellers (i.e. A200, A100, and A310 impellers) in mixing of xanthan gum solutions.

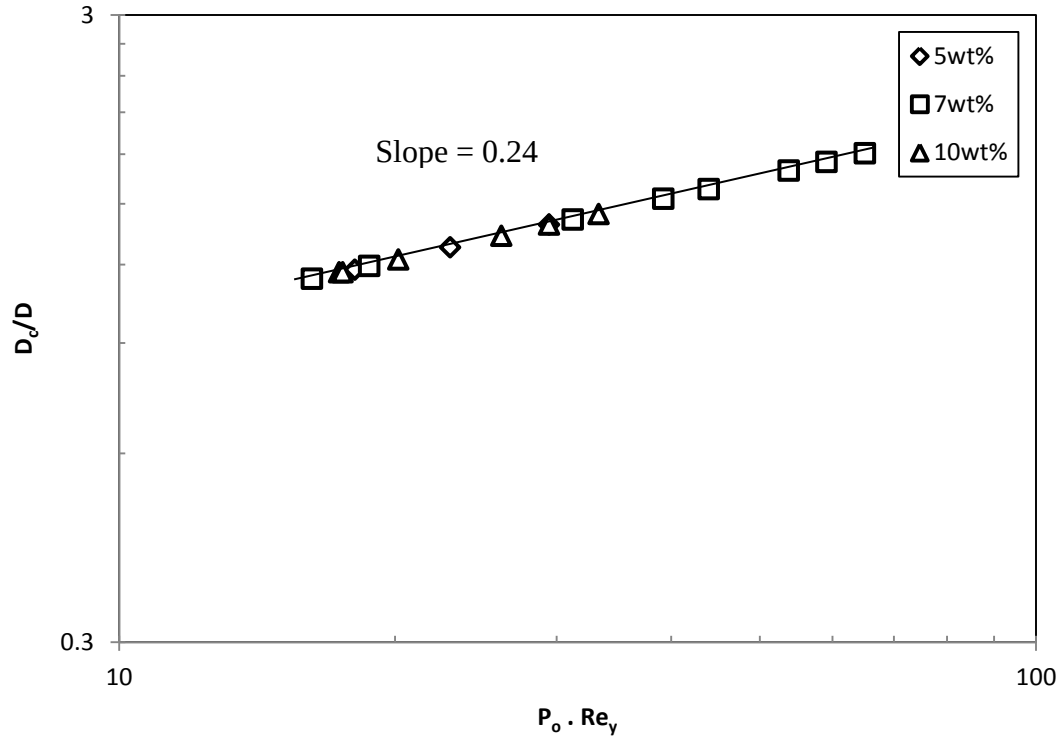

Figure 4.7. Dimensionless cavern diameter versus dimensionless stress (P_oRe_y) for 5, 7, and 10 wt% wheat straw slurry (≤ 2 mm) agitated by the A100 impeller

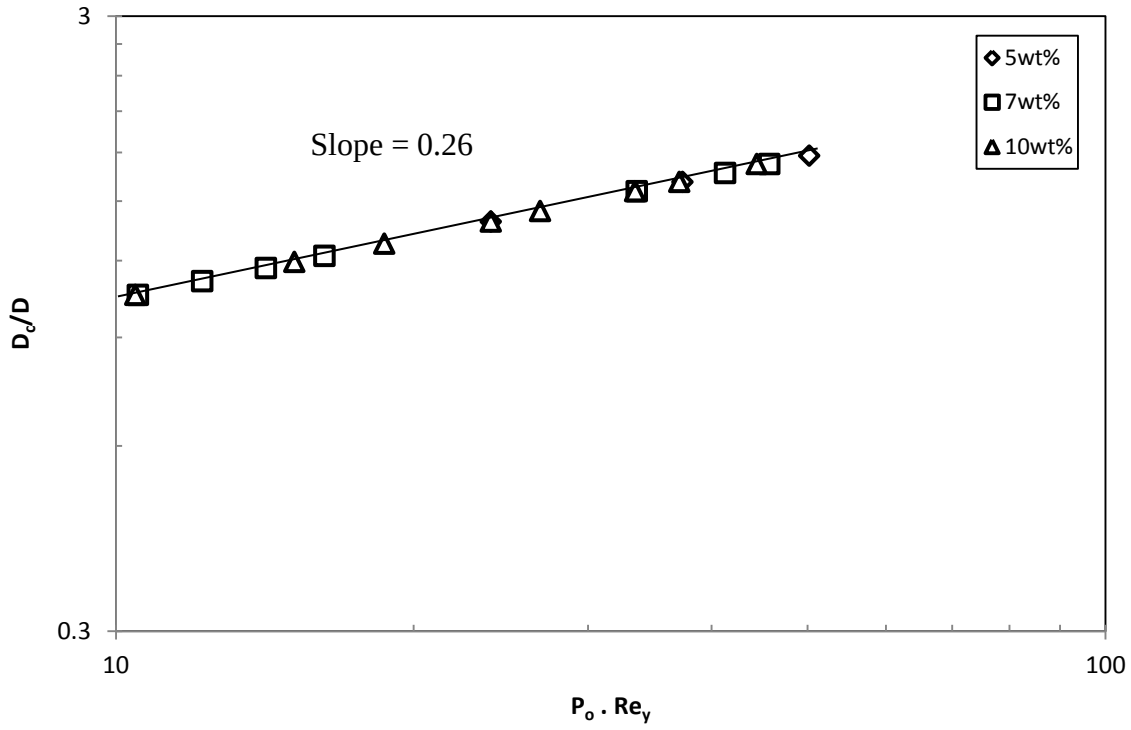

Figure 4.8. Dimensionless cavern diameter versus dimensionless stress (P_oRe_y) for 5, 7, and 10 wt% wheat straw slurry (≤ 2 mm) agitated by the A200 impeller

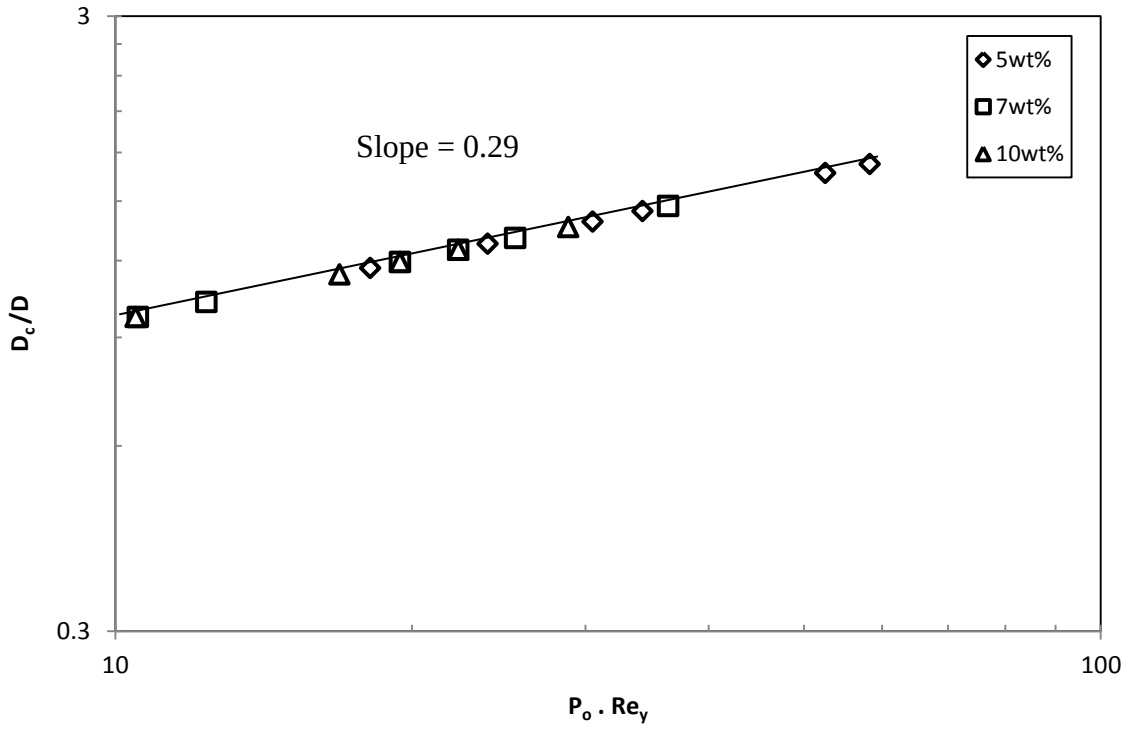

Figure 4.9. Dimensionless cavern diameter versus dimensionless stress (P_oRe_y) for 5, 7, and 10 wt% wheat straw slurry (≤ 2 mm) agitated by the A310 impeller

4.2.3 Cavern Height to Diameter Ratio (H_c/D_c)

Before the cavern touches the wall, the ratio of cavern height to cavern diameter (H_c/D_c) remains almost constant versus the impeller speed for each type of impellers (Figures 4.10 to 4.15 show (H_c/D_c)), when mixing of 5, 7, and 10 wt% wheat straw slurries of fiber sizes ≤ 2 mm and 8 mm. It can be seen that the cavern height to cavern diameter ratios were constant at 0.78, 0.57, and 0.82 for the A100, A200, and A310 impellers, respectively. These results were in good agreement with those reported in the literature for these three types of impellers as demonstrated in Table 4.1.

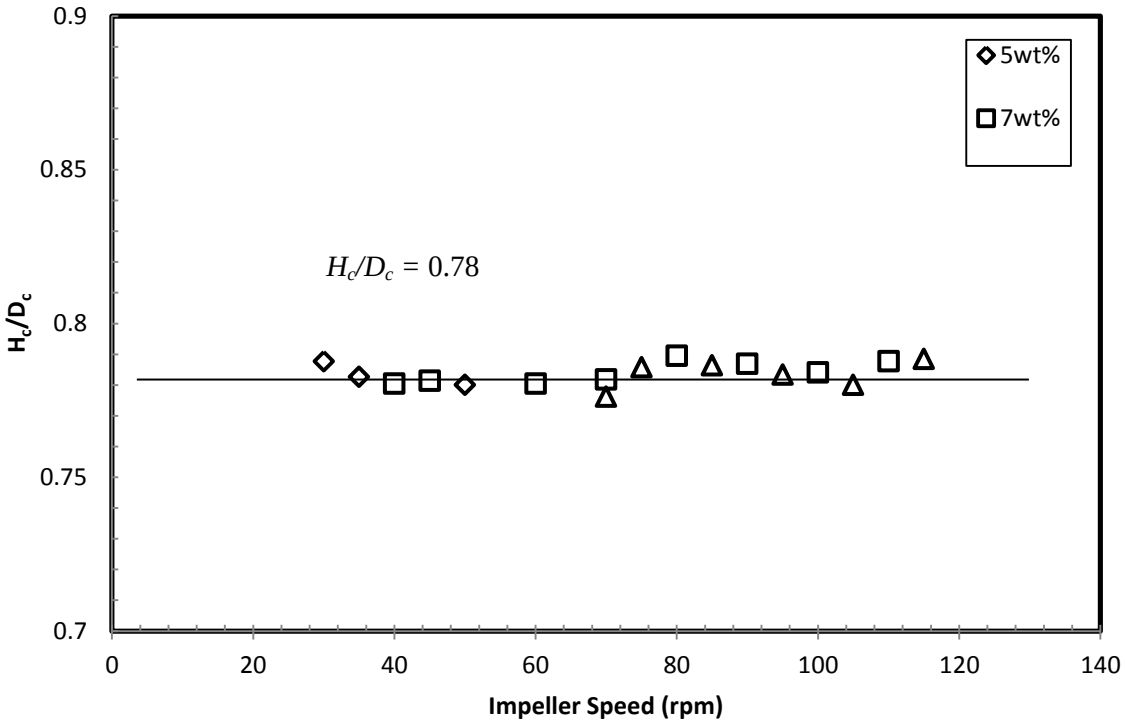

Figure 4.10. H_c/D_c versus the impeller speed for the A100 impeller, at 5, 7 and 10 wt% wheat straw slurries (≤ 2 mm)

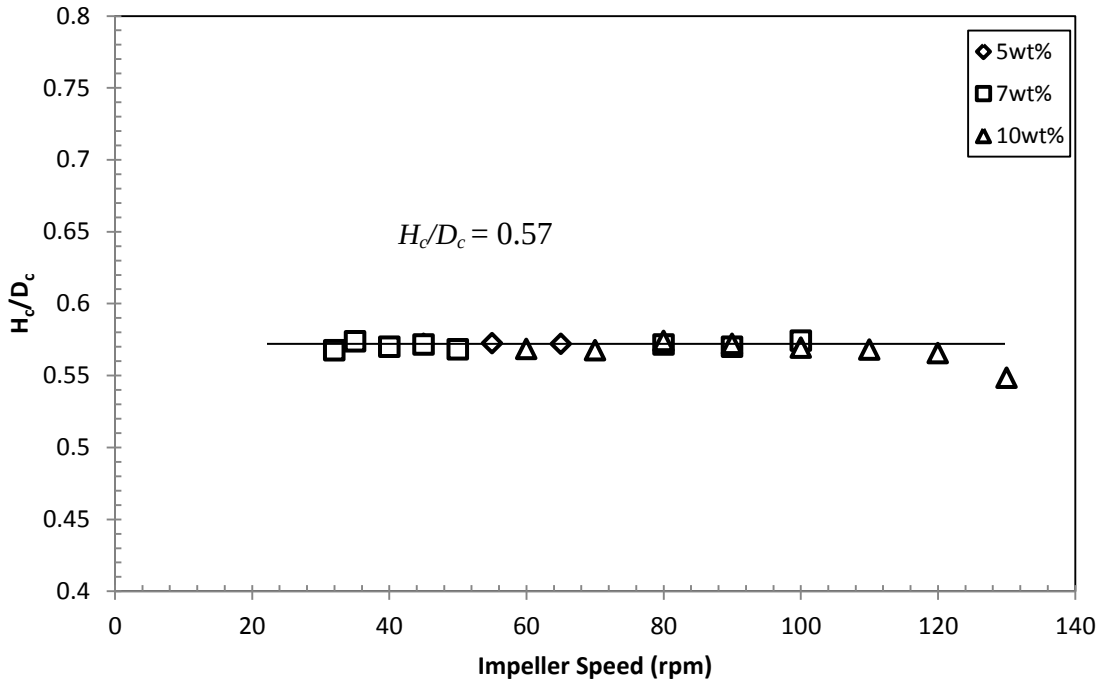

Figure 4.11. H_c/D_c versus the impeller speed for the A200 impeller, at 5, 7 and 10 wt% wheat straw slurries ($\leq$ 2 mm)

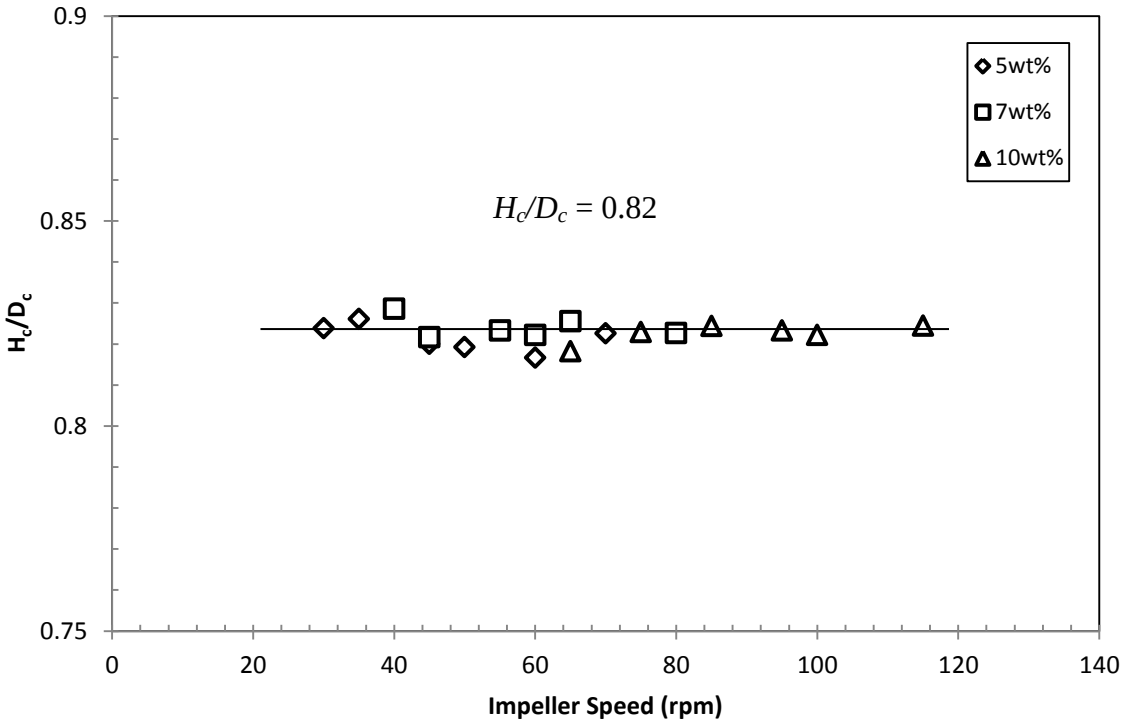

Figure 4.12 . H_c/D_c versus the impeller speed for the A310 impeller, at 5, 7 and 10 wt% wheat straw slurries (≤ 2 mm)

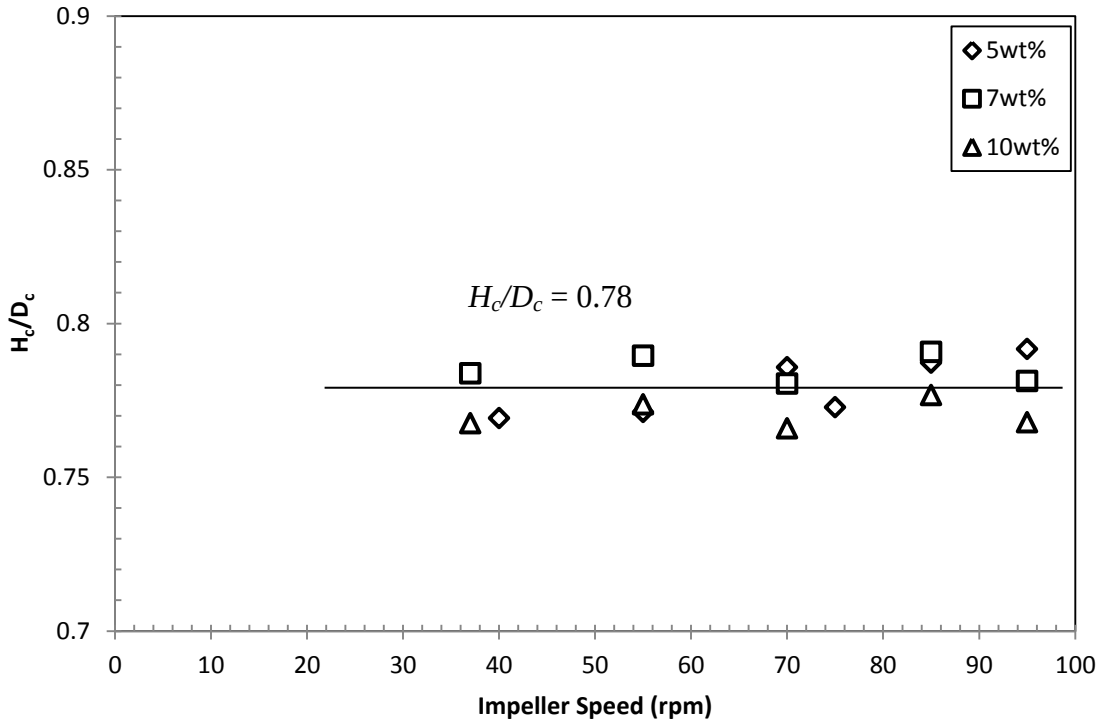

Figure 4.13. H_c/D_c versus the impeller speed for the A100 impeller, at 5, 7 and 10 wt% wheat straw slurries (8 mm)

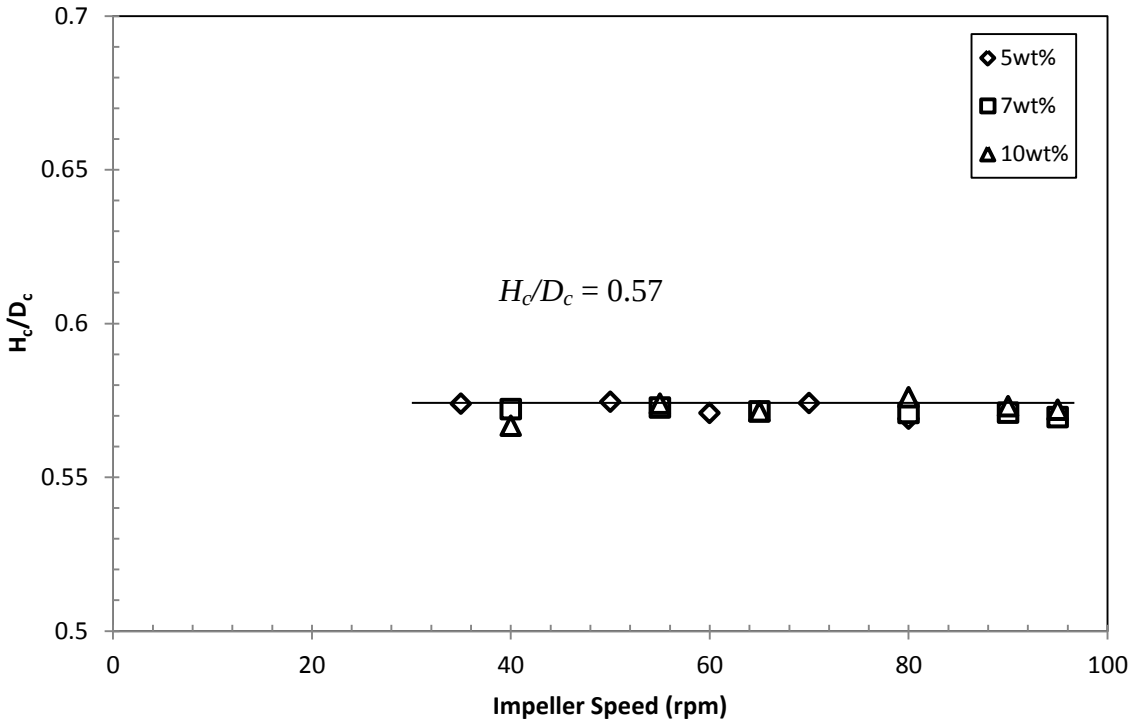

Figure 4.14. H_c/D_c versus impeller speed for the A200 impeller, at 5, 7, and 10 wt% wheat straw slurries (8 mm)

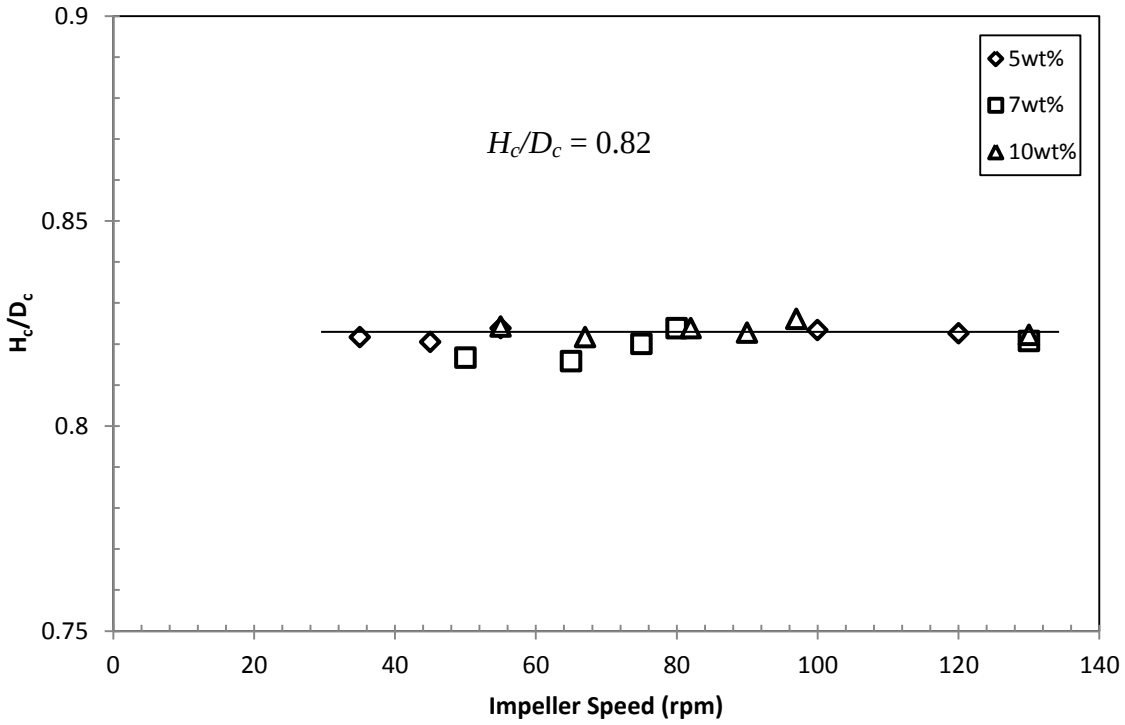

Figure 4.15. H_c/D_c versus impeller speed for the A310 impeller, at 5, 7, and 10 wt% wheat straw slurries (8 mm)

Table 4.1. H_c/D_c for the A310, A100, and A200 in agitation of non-Newtonian fluids

Impeller type	Reference	H_c/D_c
A100	Saeed *et al*., 2008 Elson, 1988 Solmon *et al*., 1981	0.75
A200	Saeed *et al*., 2008 Elson, 1988 Solomon *et al*., 1981	0.55
A310	Patel, 2012 Saeed *et al*., 2008 Elson, 1988 Solmon *et al*., 1981	0.78-0.8

4.3 *Effect of Impeller Speed on Cavern Diameter*

In order to see the effect of impeller speed on the cavern diameter, two illustrative tomograms (as a sample of obtained tomograms) are shown in Figure 4.16. This figure shows the effect of impeller speed when it was varied from 70 rpm to 95 rpm, on the diameter of the cavern for 10 wt% wheat straw slurry (≤ 2 mm) agitated by A100 impeller. These images were obtained from tomography plane 3, which was located at the impeller position. These tomograms clearly show that the diameter of the cavern increased when the impeller speed increased to 95 rpm. Similar trends were also observed for other cases.

(a) Impeller speed: 70 rpm **(b)** Impeller speed: 95 rpm

Figure 4.16. Effect of impeller speed on the diameter of the cavern for 10 wt% wheat straw slurries (≤ 2 mm) agitated by the A100 impeller for (a) 70 rpm and (b) 95 rpm

4.4 *Effect of Impeller Type on Cavern Diameter*

Figure 4.17 shows tomograms obtained from plane 3 for the A310, A200, and A100 at the rotational speed of 40 rpm and 7 wt% wheat straw slurry (≤ 2 mm). The results show the cavern diameter of 18.5 cm, 21 cm, and 21.5 cm for A310, A200, and A100, respectively.

The larger cavern diameter created by the A100 impeller and A310 resulted in the smallest cavern.

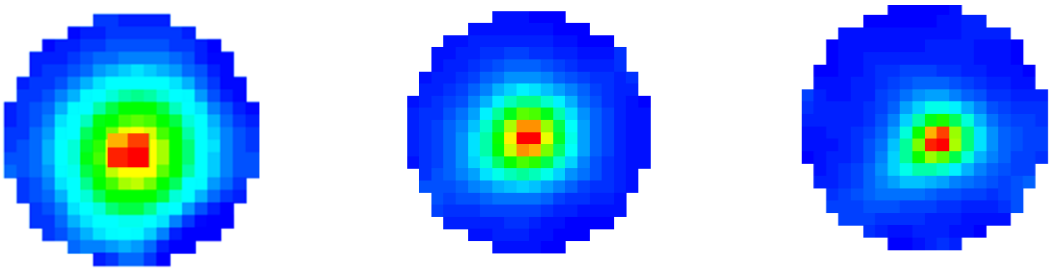

(a) A100 Impeller **(b)** A200 Impeller **(c)** A310 Impeller

Figure 4.17. Tomograms obtained from plane 3 at 7 wt% wheat straw slurries (≤ 2 mm) for (a) A100, (b) A200 and (c) A310, at 40 rpm

4.5 *Predicted Yield Stress of Wheat Straw Slurries Using Tomography Data*

The yield stress of wheat straw suspensions for concentrations of 5, 7, 10 wt% and two fiber sizes were estimated using the cylindrical model of Elson (Equation 1.11). The term $N^2D^2\rho/\tau_y$ on the right hand side of Equation (1.11) refers to the yield stress Reynolds number (Re_y) (Etchells *et al*., 1987).

As explained in the previous section, the diameter and height of the cavern were determined through ERT. These dimensions as well as the impeller speed and the power number were substituted into Equation (4.2) to obtain the slurry yield stress. The yield stresses calculated using three impellers at three concentrations (5, 7, and 10 wt%) for two fiber sizes (≤ 2 mm and 8 mm) are listed in Tables 4.2 and 4.3. It can be seen that the average yield stress for the fiber size of ≤ 2 mm at 5, 7, and 10 wt% were 1.3, 4.2, and

14.8 Pa, respectively. For the fiber size of 8 mm, the average yield stress was 3.4, 6.8, and 16.7 Pa for 5, 7, and 10 wt% concentrations, respectively.

Table 4.2. Yield stress of the wheat straw slurries for the fiber size of ≤ 2 mm calculated from cavern diameter and height

Impeller type	**[Wheat straw suspension]**	**Yield Stress (Pa)**
A100	5 wt%	1.41 ± 0.05
	7 wt%	4.05 ± 0.03
	10 wt%	15.07 ± 0.04
A200	5 wt%	1.35±0.04
	7 wt%	4.13±0.04
	10 wt%	14.70±0.08
A310	5 wt%	1.19±0.05
	7 wt%	4.37±0.07
	10 wt%	14.68±0.07

Table 4.3. Yield stress of the wheat straw slurries for the fiber size of 8 mm calculated from cavern diameter and height

Impeller type	[Wheat straw suspension]	Yield Stress (Pa)
A100	5 wt%	3.45±0.06
	7 wt%	6.76±0.05
	10 wt%	16.58±0.05
A200	5 wt%	3.46±0.09
	7 wt%	6.46±0.05
	10 wt%	16.68±0.29
A310	5 wt%	3.19±0.05
	7 wt%	6.61±0.03
	10 wt%	17.02±0.04

4.5.1 Effect of Fiber Length on Yield Stress

As shown in Tables 4.5 and 4.6 , the yield stress of the wheat straw slurry with a fiber size of 8 mm was more than that for a fibre size of ≤ 2 mm, at all three concentrations. When the fiber size increases the fibrous network will be stronger, thus the yield stress will increase.

This result is in agreement with those reported in the literature. Samaniuk *et al*. (2011) observed that the yield stress of concentrated lignocellulosic biomass (corn stover) increased with particle length. In another study, Viamajala *et al*. (2009) reported that acid

hydrolyzed corn stover slurries behaved like yield stress fluids, at various concentrations, and that with increasing particle size, the yield stress increased. Bashir (2008) measured the rheological properties of wheat straw suspension at concentrations between 5.0-20.0 wt%. The yield stress was found to increase with the size of the wheat straw fibers. Rosgaard *et al*. (2007) investigated the effect of solids content and enzymatic hydrolysis on the apparent viscosity of barley straw biomass slurries, with solids fraction varying from 5 wt% to 15 wt%. They showed that the apparent viscosity increased with solids fraction. Pimenova and Hanley (2003 and 2004) measured the apparent rheological properties of corn stover suspensions of 5, 10, 20, and 30 wt% and showed that the viscosity and the yield stress of the suspensions enhanced as the fiber size increased.

4.5.2 Effect of Fiber Mass Concentration on Yield Stress

Several studies have been conducted to relate the yield stress (τ_y) as a function of the mass concentration (C_m) in both pulp and biomass suspensions (Bennington *et al*., 1990; Dalpke and Kerekes, 2005; Knutsen and Liberatore, 2009; Stickel *et al*., 2009; Hue *et al*., 2009).

As was shown in Tables 4.5 and 4.6, by increasing fiber concentration, due to the fiber network strength the amount of yield stress is increased, which is in good agreement with Chaussy *et al*. (2011), Derakhshandeh *et al*. (2010b), and Bashir (2008) studies.

4.6 *Power Number versus Yield Stress Reynolds Number*

Typically, the power consumption of an impeller is presented using the power curve: power number versus Reynolds number. Since, in this study, we measured the yield stress of the wheat straw slurry, the yield stress Reynolds number (Equation 4.3), which is a function of the yield stress, was employed instead of Reynolds number.

$$Re_y = \left(\frac{N^2 D^2 \rho}{\tau_y}\right) \tag{4.3}$$

Figures 4.18, 4.19, and 4.20 illustrate the power number versus the yield stress Reynolds number for A100, A200, and A310 impellers.

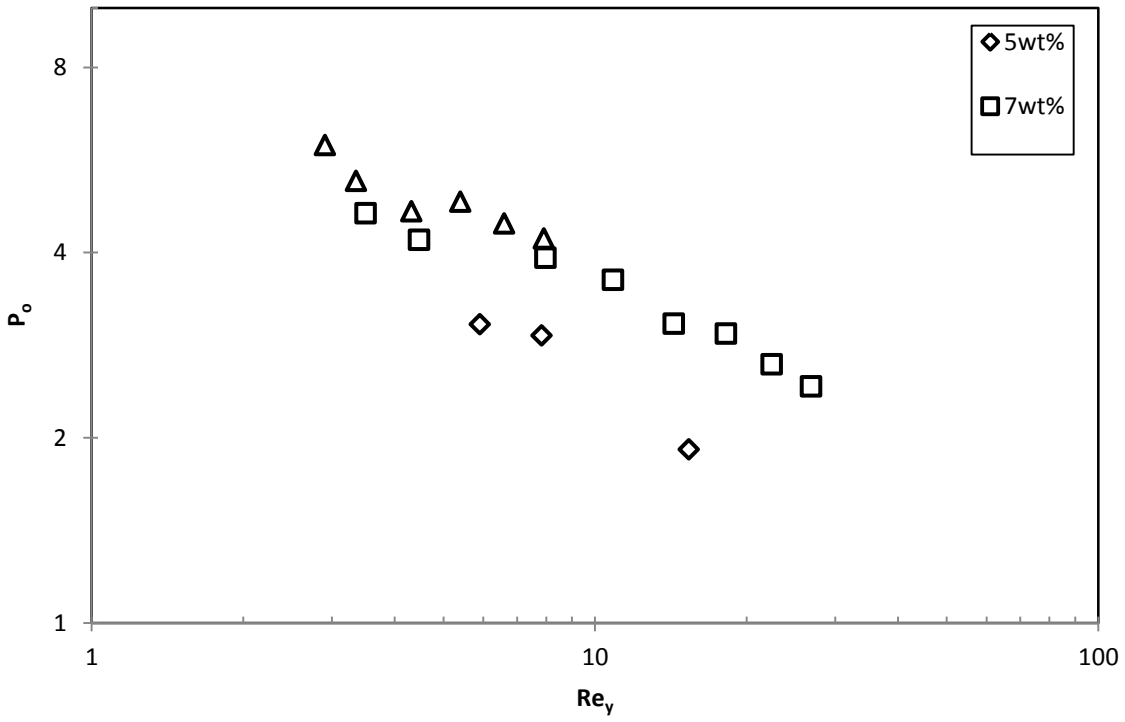

Figure 4.18. Power number versus yield stress Reynolds number for the A100 impeller and the fiber size of ≤ 2 mm

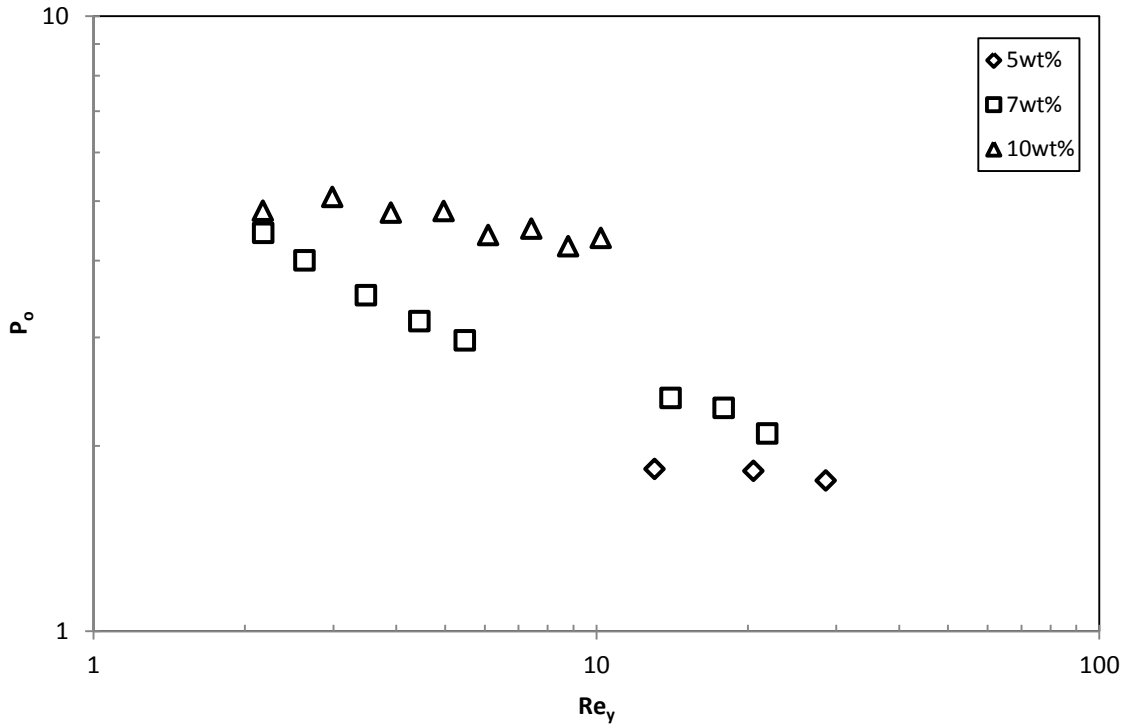

Figure 4.19. Power number versus yield stress Reynolds number for the A200 impeller and the fiber size of $\leq$2 mm

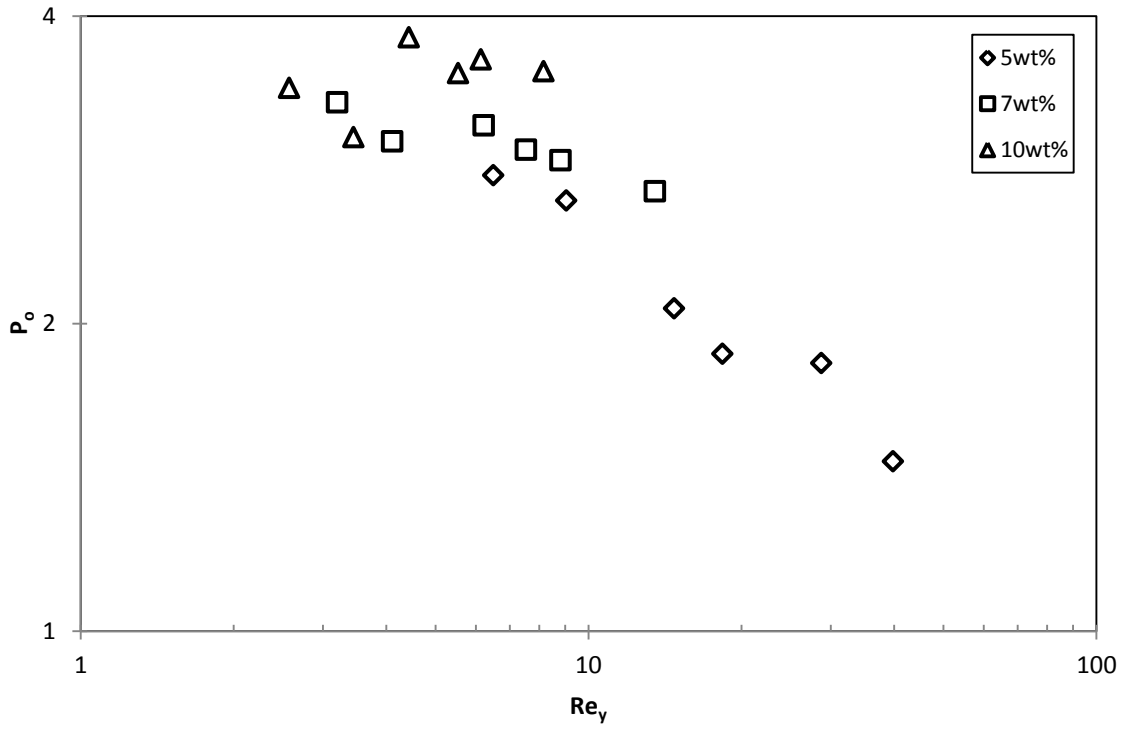

Figure 4.20. Power number versus yield stress Reynolds number for the A310 impeller and the fiber size of $\leq$2 mm

These data show that the power number of the A100 impeller was the highest among the impellers employed in this study. These figures also show that the power number increased while the concentration of wheat straw slurry increased. It should be mentioned that yield stress Reynolds number decreased when the wheat straw slurry concentration increased.

CHAPTER 5
CONCLUSION AND RECOMMENDATIONS

5.1 *Conclusion*

Electrical resistance tomography (ERT) was used to measure the cavern diameter (2D) and cavern height (3D) in the mixing of non-Newtonian wheat straw slurries with yield stress, for the A100, A200, and A310 impellers.

In this study for the first time wheat straw slurry yield stress was estimated from the cavern size obtained from ERT tomograms for three concentrations of wheat straw slurry (5,7, and 10 wt%) and two sizes of fiber ($\leq$ 2 mm 8 $\pm$ 0.014 mm) with three types of axial impellers (A100, A200, and A310) . The average yield stress of wheat straw slurries at 5, 7, and 10 wt% were 1.31 Pa, 4.2 Pa, and 14.8 Pa, respectively for the fiber size of $\leq$ 2 mm and were 3.4 Pa, 6.8 Pa, and 16.7 Pa, respectively for the fiber size of 8 mm. As expected, these values were irrespective of the type of impeller. As the slurry concentration and fiber size increased, the yield stress of the slurry also increased due to a stronger fibrous network structure.

Analysis using the 2D images at different slurry concentrations showed that the diameter of the cavern increased when the impeller speed increased for the three impellers, and that the highest ratio of the cavern height to the cavern diameter was achieved by using the A310 impeller.

5.2 *Recommendations for Future Work*

The results from experimental work in this study drew attention to areas for future considerations, as follows:

- Using computational fluid dynamics (CFD) to study the mixing of wheat straw slurries.
- Studying the performance of other mixing systems (e.g. the combination of a radial and an axial flow impellers, and the combination of a close clearance impeller and a central impeller) in the mixing of wheat straw slurries.
- Studying the rheological behavior of wheat straw slurry using the rheometry techniques.
- Exploring the mixing of other types of agricultural wastes used for the production of bioethanol.
- Assessing the effect of pre-treatment on the mixing of agricultural wastes.

Nomenclature

C_m	Mass concentration
D	Impeller diameter (m)
D_c	Cavern diameter (m)
F_a	Axial Force (N m)
g	Gravitational acceleration, (m/s^2)
H	Fluid height in the vessel (m)
H_c	Cavern height (m)
K	Consistency index ($Pa\ s^n$)
k_S	Metzner-Otto constant (-)
M	Torque (N m)
n	Power-law index (-)
N	Impeller rotational speed (s^{-1})
N_f	Axial force number
n_e	Number of electrodes (-)
P	Power (W)
P_o	Power number (-)
P1-P4	Plane number (-)
T	Tank diameter (m)
V_c	Cavern volume (m^3)

Greek Letters

$\dot{\gamma}$	Shear rate (s^{-1})
$\dot{\gamma}_{avg}$	Average shear rate (s^{-1})
η	Apparent viscosity (Pa s)
ρ	Fluid density (kg m^{-3})
τ_s	Shear stress (Pa)
τ_y	Fluid yield stress (Pa)
μ	Fluid viscosity (Pa S)
σ_{mc}	Conductivity (mS/cm)

Abbreviations

2D	Two-dimensions
3D	Three-dimensions
ADC	Analogue to digital converter
AFEX	Ammonia fiber expansion
CFD	Computational fluid dynamics
CPU	Central processing unit
DAC	Digital analogue converter
DAS	Data acquisition system
DM	Dry solids matter
DP	Degree of polymerization
ERT	Electrical resistance tomography

LDA	Laser Doppler anemometer
HWA	Hotwired anemometer
MUX	Multiplexer
PEPT	Positron emission particle tracking
SSF	Simultaneous saccharification and fermentation
UDV	Ultrasonic Doppler Velocimetry

Dimensionless Numbers

Fr	Froude number
P_o	Power number
Re	Reynolds number

Appendix

Sample of Yield Stress Calculations for a 5 wt% Wheat Straw Slurry

Cavern dimensions were measured using ERT. For each impeller speed, the experiment was repeated 3 times. Table A.1 and A.2 show the average of cavern diameter and height measurement for each speed.

Table A.1. Cavern diameter average calculated for 5 wt% wheat straw slurry (≤ 2 mm) agitated by A200 impeller at 30, 55 and 70 rpm

Impeller Speed (rpm)	Cavern Diameter (m) (Run 1)	Cavern Diameter (m) (Run 2)	Cavern Diameter (m) (Run 3)	Cavern Diameter (m) (Average)
30	0.26	0.25	0.25	0.25 ± 0.005
55	0.29	0.29	0.30	0.29 ± 0.005
70	0.32	0.31	0.33	0.32 ± 0.01

Table A.2. Cavern height average calculated for 5 wt% wheat straw slurry (≤ 2 mm) agitated by A200 impeller at 30, 55 and 70 rpm

Impeller Speed (rpm)	Cavern Height (m) (Run 1)	Cavern Height (m) (Run 2)	Cavern Height (m) (Run 3)	Cavern Height (m) (Average)
30	0.14	0.15	0.14	0.14 ± 0.005
55	0.16	0.16	0.17	0.16 ± 0.005
70	0.18	0.17	0.19	0.18 ± 0.01

Yield stress values, as shown in Table A.3., were calculated according to the steps presented after Table A.3.

Table A.3. Yield stress of 5 wt% wheat straw slurries for fiber size ≤ 2 mm, agitated by A200 impeller at 30, 55 and 70 rpm

N (rpm)	N (rps)	M (N.m)	P (J/s)	D (m)	ρ (kg/m^3)	P_0 (-)	D_c (m)	H_c (m)	τ_y (Pa)	$\tau_{y,\,ave}$ (Pa)
30	0.500	0.031	0.097	0.18	1000	4.123	0.250	0.143	1.395	1.350 ± 0.04
55	0.916	0.046	0.264	0.18	1000	1.820	0.290	0.164	1.325	
70	1.166	0.062	0.454	0.18	1000	1.514	0.320	0.183	1.330	

Step by step calculations for N = 30 rpm:

1. Value of "N" (impeller speed) was measured using a tachometer; the value was read in revolutions per minute (rpm) and then converted to revolutions per second (rps). For N = 30 rpm, N = $30/60$ = 0.5 rps
2. Value of "M" (impeller torque) was measured using a torque meter in N.m. At N=30 rpm, M was read as 0.031 N.m
3. Value of P (impeller power) was calculated using equation (3.1)

$$P = 2\pi NM = 2 \times 3.14 \times 0.5 \times 0.031 = 0.097 \text{ J/s}$$

4. Value of "D" (impeller diameter) for A200 was D = 0.18 m
5. The density of the slurry was assumed constant at ρ = 1000 kg/m^3
6. P_o (power number) was calculated using equation (1.5)

$$P_0 = \frac{P}{\rho N^3 D^5} = \frac{0.097}{1000 \times 0.5^3 \times 0.18^5} = 4.123$$

7. Value of yield stress was calculated by re-arranging equation (1.11)

$\left(\frac{D_c}{D}\right)^3 = \left[\frac{1}{\left({}^{H_c}/_{D_c} + {}^{1}/_{3}\right)\pi^2}\right]\left(\frac{N^2 D^2 \rho}{\tau_y}\right) P_0$, to give

$$\tau_y = \frac{N^2 D^2 \rho P_0}{\left(\frac{H_c}{D_c}+\frac{1}{3}\right)\pi^2}\left(\frac{D}{D_c}\right)^3 = \frac{0.5^2 \times 0.18^2 \times 1000 \times 4.123}{\left(\frac{0.143}{0.250}+\frac{1}{3}\right)\pi^2}\left(\frac{0.18}{0.250}\right)^3 = 1.395\ Pa$$

8. Standard deviation for the yield stress is calculated using

$$\sigma = \sqrt{\frac{1}{N}\sum_{i=1}^{N}\left(\tau_{y,i} - \overline{\tau_y}\right)^2}$$

where N is the number of measurements, $\tau_{y,i}$ is the yield stress measurement for sample i and $\overline{\tau_y}$ is the mean value of the yield stress measurements. So,

$$\sigma = \sqrt{\frac{1}{N}\sum_{i=1}^{N}\left(\tau_{y,i} - \overline{\tau_y}\right)^2} = \sqrt{\frac{1}{3}[(1.395 - 1.350)^2 + (1.325 - 1.350)^2 + (1.330 - 1.350)^2]}$$

$$\sigma = \sqrt{\frac{1}{3}[(0.002025) + (0.000625) + (0.000400)]} = \sqrt{\frac{1}{3}[0.003050]} = 0.031885\ Pa$$

The margin of error, at 95 percent confidence level, was calculated using

$$\mp 1.96\ \frac{\sigma}{\sqrt{N}} = \mp 1.96\ \left(\frac{0.031885}{\sqrt{3}}\right) = \mp 1.96\ (0.018409) = \mp 0.04\ Pa$$

References

Abdullah M.Z. "Electrical impedance tomography for imaging conducting mixtures in hydrocyclone separators." PhD Dissertation, University of Manchester, 1993.

Adams, L.F., A. Chiti, S. Guida, A.W. Jaffer, and M. Barigou. "Position emission particle tracking inside caverns formed during mixing of industrial slurry." *Sixth International Symposium on Mixing in Industrial Process Industries*, Niagara Falls, Ontario, August 17-21, 2008.

Adams, L.W., and M. Barigou. "CFD analysis of caverns and pseudo-caverns developed during mixing of non-Newtonian fluids." *Chemical Engineering Research and Design* 85, 2006: 598-604.

Alvira, P., M.J. Negro, and M. Ballesteros. "Effect of endoxylanase and arabinofuranosidase supplementation on the enzymatic hydrolysis of steam exploded wheat straw." *Bioresource Technology* 102, 2011: 4552-4558.

Amanullah, A., S.A. Hjorth, and A.W. Nienow. "A new mathematical model to predict cavern diameters in highly shear thinning, power law liquids using axial flow impellers." *Chemical Engineering Science* 53(3), 1998: 455-469.

Arratia, P.E., J. Kukura, J. Lacombe, and F.J. Muzzio. "Mixing of shear-thinning fluids with yield stress in stirred tanks." *AIChE Journal* 52(7), 2006: 2310-2322.

Bakker, A., and L.E. Gates. "Properly choose mechanical agitators for viscous liquids ." *Chemical Engineering Progress* 91, 1995: 25-34.

Banerjee, G., S. Car, M.S. Borrusch, N. Aslam, and J.D. Walton. "Rapid optimization of enzyme mixtures for deconstruction of diverse pretreatment/biomass feedstock combinations." *Biotechnology and Biofuels* 3(22), 2010:1-15.

Banerjee, G., S. Car, M.S. Borrusch, N. Aslam, and J.D. Walton. "Synthetic enzyme mixtures for biomass deconstruction: production and optimization of a core set." *Biotechnology Bioengineering* 106, 2010: 707-720.

Barber, C.D., B.H. Brown, and I.L. Freeston. "Imaging spatial distributions of resistivity using applied potential tomography." *Electronics Letters,* 19, 1983: 933-935.

Bart, C.H., J.J. Venneker, and H. Derksen. "Turbulent flow of shear-thinning liquids in stirred tanks-The effects of Reynolds number and flow index." *Chemical Engineering Research and Design* 8, 2010: 827-843.

Bashir, R. "Yield stress of concentrated wheat straw suspensions." M.A.Sc Thesis, Ryerson University, 2008.

Beck, M.S., E. Campogrande, M.A. Morris, R.A. Williams, and R. Waterfall. *Tomography Techniques and Processes Design and Operation*. Boston, Computational Mechanics Publications, 1993.

Bennington, C.P.J., R.J. Kerekes, and J.R. Grace. "The yield stress of suspensions" *Canadian Journal of Chemical Engineering* 68(10), 1990: 748–757.

Berlin, A., V. Maximenko, N. Gilkes, and J. Saddler. "Optimization of enzyme complexes for lignocellulose hydrolysis." *Biotechnology and Bioengineerig* 97, 2007: 287-296.

Bhole, M.R., and C.P.J. Bennington. "Performance of four axial flow impellers for agitation of pulp suspensions in a laboratory-scale cylindrical stock chest." *Industrial Engineering Chemical Research* 49, 2010: 4444-4451.

Bhole, M.R., L.K. Hui, C. Gomez, C.P.J. Bennngton, and G.A. Dumont. "The effect of off-wall clearance of a side-entering impeller on the mixing of pulp suspensions in a cylindrical stock chest." *Canadian Journal of Chemical Engineering* 89, 2011: 985-995.

Bruun, H. *Hot-Wire Anemometry Principles and Signal Analysis.* New York: Oxford UP, 1995.

Braun, H.J., G. Atlin, and T. Payne, *Multi-location testing as a tool to identify plant response to global climate change. In:* Reynolds, M.P. (Ed.), *Climate Change and Crop Production.* Oxfordshire: CABI, 2010.

Brydson, J.A. *Flow Properties of Polymer Melts. 2nd*. London: George Godwin, 1981.

Buranov, A.U., and G. Mazza. "Lignin in straw of herbaceous crops." *Industrial Crop Production* 28, 2008: 237-259

Chandra, R.P., R. Bura, W.E. Mabee, A. Berlin, X. Pan, and J.N. Saddler. "Substrate pretreatment: the key to effective enzymatic hydrolysis of lignocellulosics." *Advanced Biochemical Engineering* 108, 2007: 67-93.

Chang, V.S., and M.T. Holtzapple. "Fundamental factors affecting biomass enzymatic reactivity." *Applied Biochemistry and Biotechnology* 84-86, 2000: 5-37.

Chaussy, D., C. Martin, and J.C. Roux. "Rheological behavior of cellulose fiber suspensions: application to paper-making processing." *Industrial and Engineering Chemistry Research* 50, 2011: 3524-533.

Chhabra, R.P., and J.F. Richardson. *Non-Newtonian flow and applied rheology. 2nd ed.* Amsterdam: Butterworth-Heinemann, 2008.

Chiti, F., S. Bakalis, W. Bujalski, M. Barigou, A. Eaglesham, and A.W. Nienow. "Using positron emission particle tracking (PEPT) to study the turbulent flow in a baffled vessel agitated by a Rushton turbine: Improving data treatment and validation." *Chemical Engineering Research and Design* 89, 2011: 1960-1974.

Etchells A.W., W.N. Ford, and D.G.R. Short. "Mixing of Bingham plastics on an industrial scale." *Industrial Chemical Engineering Symposium* 10(8), 1987: 8-10.

Dalpke, B., and R.J. Kerekes. "The influence of fibre properties on the apparent yield stress of flocculated pulp suspensions." *Journal of Pulp and Paper Science* 31(1), 2005: 39–43.

Dasari, R., and R.E. Berson. "The effect of particle size on hydrolysis reaction rates and rheological properties in cellulosic slurries." *Applied Biochemistry and Biotechnology* 137-140(1-12), 2007: 289-299.

Derakhshandeh, B., S.G. Hatzikiriakos, and C.P.J. Bennington. "Rheology of pulp fibre suspensions using ultrasonic Doppler velocimetry." *Rheological Acta* 49(11-12), 2010a: 1127-1140.

Derakhshandeh, B., S.G. Hatzikiriakos, and C.P.J. Bennington. "The apparent yield stress of pulp fibre suspensions." *Journal of Rheology* 54(5), 2010b: 1137-1154.

Dickin, F., and M. Wang. "Electrical resistance tomography for process applications." *Measurement Science and Technology* 7(3), 1996: 247-260.

Drain, L.E., *The Laser Doppler Technique.* New York: John Wiley & Sons Ltd., 1980.

Drust, F., V. Buwa, A. Dewan, and A.F. Nasser. "Fluid dynamics and mixing of single-phase flow in a stirred vessel with a grid disc impeller: Experimental and numerical investigations." *Chemical Engineering Science* 61, 2006: 2815-2822.

Elson, T.P. "The growth of caverns formed around rotation impellers during the mixing of a yield stress fluid." *Chemical Engineering Communications* 391, 1990: 303-319.

Elson, T.P., and D.J. Cheesman. "X-Ray studies of cavern sizes and mixing performance with fluids possessing a yield stress." *Chemical Engineering Science* 41(10), 1986: 2555-2562.

Erdei, B., Z. Barta, B. Sipos, K. Reczey, M. Galbe, and G. Zacchi. "Ethanol production from mixture of wheat straw and wheat meal." *Biotechnology for Biofuels* 3(16), 2010:1-9.

Etchells, A.W., W.N. Ford, and D.G.R. Short. "Mixing of Bingham plastics on an industrial scale." *Industrial Chemical Engineering Program Symposium Series*, 108, 1987: 1-10.

Galindo, E., and Nienow A.W. "Mixing of highly viscous simulated xanthan fermentation broths with the Lightnin A-315 impeller." *Biotechnology Progress* 8(3), 1992: 223-239.

Gabelle, C ., F. Augier, A. Carvalho, R. Rousset, and J. Morchain. "Effect of tank size on kLa and mixing time in aerated stirred reactors with non-newtonian fluids." *The Canadian Journal of Chemical Engineering* 89(5), 2011: 1139-1153.

Galazka, J.M., C.G. Tian, W.T. Beeson, B. Martinez, N.L. Glass, and J.H.D. Cate. "Cellodextrin transport in yeast for improved biofuel production." *Science* 330, 2010: 84-86.

Galbe, M., and G. Zacchi. "Pretreatment of lignocellulosic materials for efficient bioethanol production." *Biofuels* 108, 2007: 41-65.

Ganesh, K., J.B. Joshi, and S.B. Sawant. "Cellulase deactivation in a stirred reactor." *Biochemical Engineering Journal* 4, 2000: 137-141.

Gil, N., S. Ferreira, M.E. Amaral, F.C. Domingues, and A.P. Duarte. "The influence of dilute acid pretreatment conditions on the enzymatic saccharification of *Erica* spp. for bioethanol production." *Industrial Crops Production* 32, 2010: 29-35.

Gisser, D.G., Issacson, D., Newell, J. "Current topics in impedance imaging." *Clinical Physics and Physiological Measurement* 8, 1987: 36-46.

Grohmann, K., R. Torget, and M. Himmel. "Optimization of dilute acid pretreatment of biomass." *Biotechnology and Bioengineering Symposium* 15, 1985: 59-80.

Guo, G.L., W.H. Chen, L.C. Men, and W.S. Hwang. "Characterization of dilute acid pretreatment of silvergrass for ethanol production." *Bioresource Technology* 99, 2008: 6046–6053.

Gurgu, L., Á. Lafraya, J. Polaina, and J . Marín-Navarro. "Fermentation of cellobiose to ethanol by industrial *Saccharomyces* strains carrying the β-glucosidase gene (BGL1) from *Saccharomycopsis fibuligera*." *Bioresource Technology* 102, 2011: 5229–5236.

Ha, S.H., N.L. Mai, G. An, and Y-M. Koo. "Microwave-assisted pretreatment of cellulose in ionic liquid for accelerated enzymatic hydrolysis." *Bioresource Technology* 102, 2011: 1214–1219.

Hagerdal, B. "Expression of the gxf1 transporter from *Candida intermedia* improves fermentation performance in recombinant xylose-utilizing *Saccharomyces cerevisiae*." *Applied Microbial Biotechnology* 82, 2009: 123–130.

Hahn-Hagerdal, B., K. Karhumaa, C. Fonseca, I. Spencer-Martins, and M.F. Gorwa-Grauslund. "Towards industrial pentose fermenting yeast strains." *Applied Microbial Biotechnology* 74, 2007: 937–953.

Hahn-Hagerdal, B., K. Karhumaa, M. Jeppsson, and M.F. Gorwa-Grauslund. "Metabolic engineering for pentose utilization in *Saccharomyces cerevisiae*." *Biofuels* 108, 2007: 147-177.

Hahn-Hagerdal, B., M. Galbe, M.F. Gorwa-Grauslund, G. Liden, and G. Zacchi. "Bioethanol – The fuel for tomorrow from the residues of today." *Trend in Biotechnology* 24(12), 2006: 541-556.

Hämäläinen, T., and J. Hämäläinen. "Modelling of fibre orientation in the headbox jet." *Journal of Pulp and Paper Science* 33, 2007: 49-53.

Herschel, W.E., and R. Bulkley. "Measurements of consistency as applied to rubber-benzene solutions." *Proceedings of the American Society of Testing Materials* 26(2), 1926: 621-633.

Himmel, M.E., S.H. Ding, D.K. Johnson, W.S. Adney, M.R. Nimlos, J.W. Brady, and T.D. Foust. "Biomass recalcitrance: engineering plants and enzymes for biofuels production." *Science* 315, 2007: 804–807.

Himmelsbach, W. "Investigation on heat and mass transfer and homogenization in agitated fermenters, on the example of xanthan." *Chemie-Ingenieur-Technik* (1985).

Hirata, Y., A.W. Nienow, and A.I. Moore. "Estimation of cavern size in a shear – thinning plastic fluid agitated by a Rushton turbine based on LDA measurements." *Journal of Chemical Engineering of Japan* 27(2), 1994.

Hirata, Y., and Y. Aoshima. "Formation and growth of cavern in yield stress fluids." *Transactions of the Institution of Chemical Engineers Part A* 74, 1996: 438-444.

Hongzhang, C., and L. Liying. "Unpolluted fractionation of wheat straw by steam explosion and ethanol extraction." *Bioresource Technology* 98, 2007: 666–676.

Hosseini, S., D. Patel, F. Ein-Mozaffari, and M. Mehrvar. "Study of solid-liquid mixing in agitated tank through electrical resistance tomography." *Chemical Engineering Technology* 23, (7), 2010: 605-613.

Huhtanen, J.P. *Modeling of fiber suspension flows in refiner and other papermaking processes by combining non-Newtonian fluid dynamics and turbulence.* Ph.D. Thesis, Tampere University of Technology, Tampere, 2004.

Hua, P., E.J. Woo, J.G. Webster, and W.J. Tompkins. "Using compound electrodes in electrical impedance tomography." *IEEE Transactions on Biomedical Engineering* 40, 1993: 29-34.

Hui, L.K., C.P.J. Bennington, and G.A. Dumont. "Cavern formation in pulp suspension using side entering axial flow impellers." *Chemical Engineering Science* 64, 2009: 509-519.

Hulsz, G., and F. Lopez-Alquicira. "Hot-wire anemometry in acoustic waves." *Experiments in Fluids* 30, 2001: 283-285.

Ihejirika, I., and F. Ein-Mozaffari. "Using CFD and ultrasonic velocimetry to study the mixing of pseudoplastic fluids with a helical ribbon impeller." *Chemical Engineering Technology* 30(5), 2007: 606-614.

Wilkens R.J., J.D. Miller, D.C. Dietz, and K.J. Myers. "New technique for measuring and modeling cavern dimensions in a Bingham plastic fluid." *Chemical Engineering Science* 60, 2005: 5269-5275.

Jaworski, Z., A.W. Nienow, and K.N. Dyster. "An LDA study of the turbulent flow field in a baffled vessel agitated by an axial, down-pumping hydrofoil impeller." *Canadian Journal of Chemical Engineering* 74, 1996: 3-15.

Jeon, E., J.E. Hyeon, L.S Eun, B.S. Park, S.W. Kim, and J. Lee. "Cellulosic alcoholic fermentation using recombinant *Saccharomyces cerevisiae* engineered for the production of *Clostridium cellulovorans* endoglucanase and *Saccharomycopsis fibuligera* β-glucosidase." *FEMS Microbiology Letters* 301, 2009: 130–136.

Jorgensen, H., J.B. Kristensen, and C. Felby. "Enzymatic conversion of lignocellulose into fermentable sugars: challenges and opportunities." *Biofuels, Bioproducts and Biorefining* 1, 2007: 119-134.

Kaminoyama, M., S. Taguchi, R. Misumi, and K. Nishi. "Monitoring stability of reaction and dispersion states in a suspension polymerization reactor using electrical resistance tomography measurements." *Chemical Engineering Science* 60, 2005: 5513-5518.

Kaparaju, P., M. Serrano, A.B. Thomsen, P. Kongjan, and I. Angelidaki. "Bioethanol, biohydrogen and biogass production from wheat straw in a biorefinery concept." *Bioresource Technology* 100, 2009: 2562–2568.

Katahira, S., M. Ito, H. Takema, Y. Fujita, T. Tanino, and T. Tanaka. "Improvement of ethanol productivity during xylose and glucose co-fermentation by xylose-assimilating *S. cerevisiae* via expression of glucose transporter sut1." *Enzyme Microbial Technology* 43, 2008: 115–119.

Kerekes, R.J., R.M. Soszynski, and P.A. Tam Doo. The flocculation of pulp fibres. *In: Papermaking Raw Materials*. Transactions of the VIIIth Fundamental Research Symposium, V. Puton, ed., *Mechanical Engineering Publication Limited*, London, 1985: 265-310.

Kim, S., A.N. Nkaya, and T. Dyakowski. "Measurement of mixing of two miscible liquids in a stirred vessel with electrical resistance tomography." *International Communication in Heat and Mass Transfer* 33, 2006: 1088-1095.

Kitagawa, T., K. Tokuhiro, H. Sugiyama, K. Kohda, N. Isono, and Hisamatsu. "Construction of a β-glucosidase expression system using the multistress-tolerant yeast *Issatchenkia orientalis*." *Applied Microbiology Biotechnology* 87, 2010: 1841–1853.

Kumar, R., and C.E. Wyman. "Effect of enzyme supplementation at moderate cellulase loadings on initial glucose and xylose release from corn stover solids pretreated by leading technologies." *Biotechnology and Bioengineering* 102, 2009: 457–467.

Lavenson, D.M., E.J. Tozzi, M.J. McCarthy, and R.L. Powell. "Yield stress of pretreated corn stover suspensions using magnetic resonance imaging." *Biotechnology and Bioengineering* 108(10), 2011: 2312-2319.

Lee, J. "Biological conversion of lignocellulosic biomass to ethanol." *Journal of Biotechnology* 56, 1997: 1-24.

Madupu, A., A. Mazumdar, Z. Jinsong, D. Roelant, and R. Srivastava. "Electrical resistance tomography for real-time mapping of the solid-liquid interface in tanks containing optically opaque fluids. *Proceedings SPIE* 5674, 36-46. 2005.

Mann, R., M.Dickin, T. Wang, R.A. Dyakowski, R.B. Williams, and A.E. Edwards. "Application of electrical resistance tomography to interrogate mixing processes at plant scale." *Chemical Engineering Science* 52, 1997: 2087–2097.

Mavros, P. "Flow visualization in stirred vessels, a review of experimental techniques." *Chemical Engineering Research and Design* 79, 2001.

McCabe, W.L., J. C. Smith, and P. Harriott. *Unit Operations of Chemical Engineering (7th edition).* New York: McGraw-Hil, 2005.

McMillan, J.D. "Pretreatment of lignocellulosic biomass**.** *In***:** *Enzymatic Conversion of Biomass for Fuels Production. ACS Symposium Series 566.*

Metzner, A.B. and R.E. Otto. "Agitation of non-Newtonian fluids." *AIChE Journal* 3(1), 1957: 3-10.

Mosie, N., C.E. Wyman, B.E. Dale, R. Elander, Y.Y. Lee, and M.T. Holtzapple. "Features of promising technologies for pretreatment of lignocellulosic biomass." *Bioresource Technology* 96, 2005: 673–686.

Nakamura, N., R. Yamada, S. Katahira, T. Tanaka, H. Fukuda, and A. Kondo. "Effective xylose/cellobiose co-fermentation and ethanol production by xylose-assimilating *S. cerevisiae* via expression of β-glucosidase on its cell surface." *Enzyme Microbial Technology* 43, 2008: 233–236.

Ohno, H., and Y. Fukaya. "Task specific ionic liquid for cellulose technology." *Chemical Letters* 38, 2009: 2–7.

Oldshue, J.Y. *Fluid Mixing Technology.* New York: McGraw-Hil, 1983.

Pakzad, L. ”Using electrical resistance tomography (ERT) and computional fluid dynamics to study the mixing of pseudoplastic fluids with a Scaba 6RGT impeller." *M.A.Sc Thesis*, Ryerson University, 2007.

Pakzad, L., F. Ein-Mozaffari, and P. Chan. "Using electrical resistance tomography and computational fluid dynamics modeling to study the formation of cavern in the mixing of pseudoplastic fluids possessing yield stress." *Chemical Engineering Science* 63, 2008: 2508–2522.

Papatheofanous, M.G., E. Billa, D.P. Koullas, B. Monties, and E.G. Koukios. "Optimizing multisteps mechanical-chemical fractionation of wheat straw components." *Industrial Crops and Products* 7, 1998: 249–256.

Prasad, S., A. Singh, and H.C. Joshi, "Ethanol as an alternative fuel from agricultural, industrial and urban residues." *Resources Conservation and Recycling* 50, 2007: 1-39.

Patel, S.J., R. Onkarappa, and S.B. Gurumurty. "Pretreatment studies of wheat straw and rice." *The Internet Journal of Microbiology* 7(1), 2009: 63-65.

Patel, D., F. Ein-Mozaffari, and M. Mehrvar. "Improving the dynamic performance of continuous-flow mixing of pseudoplastic fluids possessing yield stress using Maxblend impeller." *Chemical Engineering Research and Design* 90(4), 2012a: 514-523.

Patel, D., F. Ein-Mozaffari, and M. Mehrvar. "Effect of impeller type on continuous-flow mixing of non-Newtonian fluids in stirred vessels through dynamic tests." *Canadian Journal of Chemical Engineering* 90(2), 2012b: 290-298.

Paul, E. L., V.A. Atiemo-Obeng, and S.M. Kresta. *Hand book of Industrial Mixing : Science and Practice.* Hoboken: John Wiley and Sons, 2004.

Pettersson, J., and A. Rasmuson. "The yield stress of gas/liquid/fiber." *The Canadian Journal of Chemical Engineering* 82, 2004.

Pimenova, N., and T.R. Hanley. "Effect of corn stover concentration on rheological chracteristics." *Applied Biochemistry and Biotechnology* 7(1), 2004: 63-65.

Pimenova, N.V., and T.R. Hanley. "Measurement of rheological properties of corn stover suspensions." *Applied Biochemistry and Biotechnology* 1, 2003: 105-108.

Pinheiro, P.A.T., W.W. Loh, and F.J. Dickin. "Optimal sized electrodes for electrical resistance tomography." *Electronics Letters* 34(1), 1998: 69-70.

Rosgaard, L., S. Pedersen, and A.S. Meyer. "Comparison of different pretreatment strategies for enzymatic hydrolysis of wheat and barley straw." *Applied Biochemistry Biotechnology* 143, 2007: 284–296.

Saha, B.C., L.B. Iten, M.A. Cotta, and Y.V. Wu. "Dilute acid pretreatment, enzymatic saccharification and fermentation of wheat straw to ethanol." *Process Biochemistry* 40, 2005: 3693–3700.

Samaniuk, J.R., J. Wang, T.W. Root, C.T. Scott, and D.J. Klingenberg. "Rheology of concentrated biomass." *Korea-Australia Rheology Journal* 23(4), 2011: 237-245.

Shen, Y., Y. Zhang, T. Ma, X.M. Bao, F.G. Du, and G.Q. Zhuang. "Simultaneous saccharification and fermentation of acid-pretreated corncobs with a recombinant *Saccharomyces cerevisiae* expressing β-glucosidase." *Bioresource Technology* 99, 2008: 5099–5103.

Shervin, C. R., D.A. Raughley, and R.A. Romaszewski. "Flow visualization scaleup studies for the mixing of viscoelastic fluids." *Chemical Engineering Science* 46, 1991: 2867-2873.

Solomon, J., T.P. Elson, and A.W. Nienow. "Cavern sizes in agitated fluids with a yield stress." *Chemical Engineering Communication* 11, 1981: 143-164.

Sorensen, H.R., S. Pedersen, C.T. Jorgensen, and A.S. Meyer. "Enzymatic hydrolysis of wheat arabinoxylan by a recombinant minimal enzyme cocktail containing β-xylosidase and novel endo-1,4-β-xylanase and α-(L)-arabinofuranosidase activities." *Biotechnology Progress* 23, 2007: 100-107.

Sun, Y., and J. Cheng. "Hydrolysis of lignocellulosic materials for ethanol production: a review." *Bioresource Technology* 83, 2002: 1-11.

Swatloski, R.P., S.K. Spear, J.D. Holbrey, and R.D. Rogers. "Ionic liquids: new solvents for nonderivitized cellulose dissolution." *American Chemical Society*, 2002: 224-226.

Taherzadeh, M., and K. Karimi. "Pretreatment of lignocellulosic wastes to improve ethanol and biogas production." *Bioresource Technology* 10(17), 2007: 7879-7886.

Tahvildarian, P., "Using electrical resistance tomography to characterize and optimize the mixing of micron sized polymetric particles in a slurry reactor." *M.A.Sc Thesis*, Ryerson University, 2010.

Talebnia, F., D. Karakashev, and I. Angelidaki. "Production of bioethanol from wheat straw: An overview on pretreatment, hydrolysis and fermentation." *Bioresource Technology* 101(13), 2010: 4744-4753.

Tattersan, G.B. "Scaleup and design of industrial mixing processes." *AIChE Journal* 41(3), 1994: 741-758.

Thring, R., and M.F. Edwards. "An experimental investigation into the complete suspension of floating solids in an agitated tank." *Industrial Engineering Chemical Research* 29, 1990: 676-682.

Valjamae, P., V. Sild, G. Pettersson, and G. Johansson. "The initial kinetics of the hydrolysis by cellobiohydrolases I and II is consistent with a cellulose surface-erosion model." *European Journal of Biochemistry* 253, 1998: 469–475.

Viergever M.A., and A.E. Todd-Pokropek. "*Mathematics and Computer Science in Medical Imaging*." Berlin: Springer, 1988.

Visuri, O., M. Laakkonen, and J. Aittamaa. "A digital imaging technique for the analysis of local inhomogeneities from agitated vessels." *Chemical Engineering Technology* 30(12), 2007: 1692–1699.

Vlaev, D., M. Wang, T. Dyakowski, R. Mann, and B.D. Grieve. "Detecting filter-cake pathologies in solid–liquid filtration: semi-tech scale demonstrations using electrical resistance tomography (ERT)." *Chemical Engineering Journal* 77(1), 2000: 87-91.

Wang M., X. Jia, M. Bennet, and R.A. Williams. "Flow regime identification and optimum interfacial area control of bubble columns using electrical impedance imaging." 2nd World Congress on Industrial Process Tomography, 2001: 726-727.

Watanabe, S., A. Abu Saleh, S.P. Pack, N. Annaluru, T. Kodaki, K., Makino. "Ethanol production from xylose by recombinant *Saccharomyces cerevisiae* expressing protein engineered NADP(+)-dependent xylitol dehydrogenase." *Journal of Biotechnology* 130, 2007: 316–319.

Wichterle, K., and O. Wein. "Agitation of concentrated suspensions." *CHISA* 75, 1975.

Wilkens R.J., J.D. Miller, D.C. Dietz, and K.J. Myers. "New technique for measuring and modeling cavern dimensions in a Bingham plastic fluid." *Chemical Engineering Science* 60, 2005: 5269-5275.

Williams, R.A., and M.S. Beck. *Process Tomography: Principles, Techniques and Applications.* Waltham: Butterworth-Heinemann, 1995.

Xu, F., J. Sun, R. Sun, P. Fowler, and M.S. Baird. "Comparative study of organosolv lignins from wheat straw." *Industrial Crops and Products* 23, 2006: 180-193.

Yackel, D.C. *Pulp and Paper Agitation: The History, Mechanics, and Process.* Atlanta: TAPPI Press, 1990.

Yanase, S., T. Hasunuma, R. Yamada, T. Tanaka, C. Ogino, and A. Fukuda. "Cellulase gene of termite origin." *Nature* 394, 1998: 330-331.

Yeh, Y. and H.Z. Cummins. "Localized fluid flow measurements with an He-Ne laser spectrometer." *Applied Physical Letter* 4, 1964: 176-178.

Young, E., S.M. Lee, and H. Alper. "Optimizing pentose utilization in yeast: the need for novel tools and approaches." *Biotechnology and Biofuels* 3, 2010.

Zhang, M.J., R.X. Su, W. Qi, and Z.M. He. "Enhanced enzymatic hydrolysis of lignocellulose by optimizing enzyme complexes." *Applied Biochemistry and Biotechnology* 160, 2010: 1407–1414.

Zhang, Y.H.P., S.Y. Ding, J.R. Mielenz, J.B. Cui, R.T. Elander, and M. Laser. "Fractionating recalcitrant lignocellulose at modest reaction conditions." *Biotechnology and Bioengineering* 97, 2007: 214–223.

Zhao, H., C.L. Jones, G.A. Baker, S. Xia, O. Olubajo, and V.N. Person. "Regenerating cellulose from ionic liquids for an accelerated enzymatic hydrolysis." *Journal of Biotechnology* 139, 2009: 47-54.

Zhao, Z.F., M. Mehrvar, and F. Ein-Mozaffari. "Mixing time in an agitated multi-lamp cylindrical photoreactor using electrical resistance tomography." *Journal of Chemical Technology and Biotechnology* 83, 2008: 1676-1688.

Zhu, S.D., Y.X. Wu, Q.M. Chen, N. Yu, C.W. Wang, and S.W. Jin. "Dissolution of cellulose with ionic liquids and its application: a mini-review." *Green Chemistry* 8, 2006: 235-237.

Zhu, Z.G., N. Sathitsuksanoh, T. Vinzant, D.J. Shell, J.D. McMillan, and Y-H.P. Zhang. "Comparative study of corn stover preteated by dilute acid and cellulose solvent-based lignocellulose fractionation: enzymatic hydrolysis, supramolecular structure, and substrate accessibility." *Biotechnology and Bioengineering* 103, 2009: 715-724.